July 2014
Volume 120
Issue 1939
£5.10

www.electronicsworld.co.uk

Electronics WORLD

THE ESSENTIAL ELECTRONICS ENGINEERING MAGAZINE

Turning lead times into transit times

by Digi-key

Technology
New material will improve transistors in electronic devices

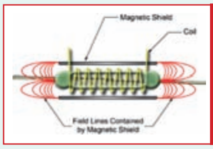

Electronic Components
Reed relay basics

Event
ECOC 2014

Cover supplied by
DIGI-KEY CORPORATION
More on pages 8-9

14

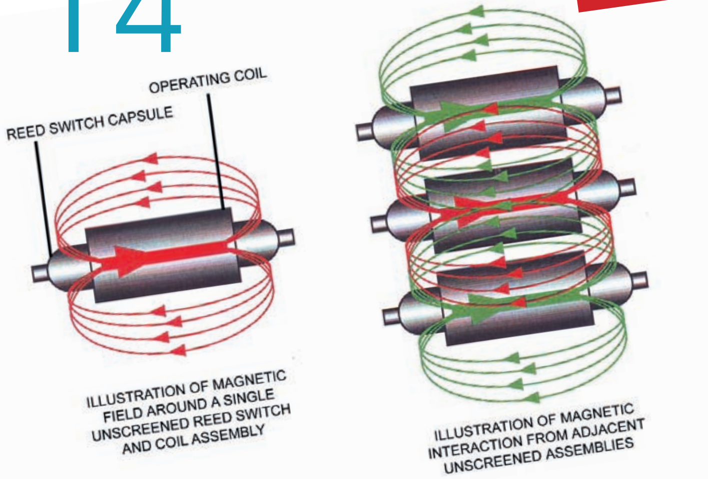

REGULARS

06

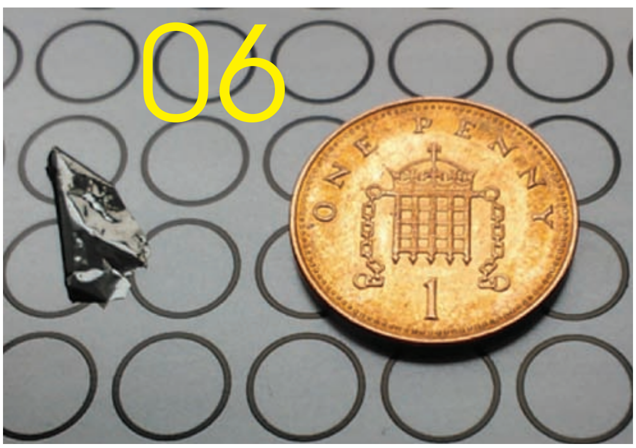

FEATURES

12

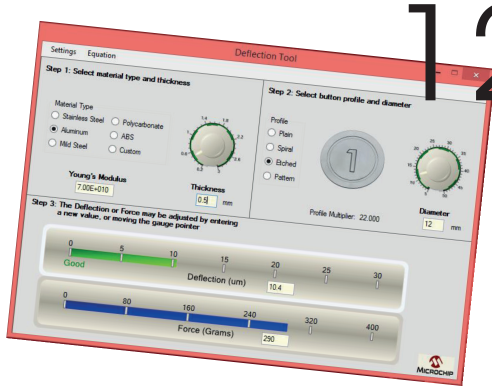

WEARABLE TECHNOLOGY $50bn INVESTMENT FRENZY

> Market specialist IDTechEx predicts that as many as 55 billion IoP devices will be in use in 2025, many employing printed, flexible electronics and completely new components

Many electronics companies, computer service providers and various conglomerates have huge amounts of funds available for investment to counter their saturating sales in mature markets. Among the companies with several billion dollars lying in the bank are Samsung, General Electric, Google and Apple, with the latter having a staggering $133bn it can tap into immediately. They all seek the "next big thing", or potentially-huge emerging markets to get involved in. Wearable technology is one of them, attracting close attention. Google Trends has a graph headed steeply upwards depicting the interest in this technology of several companies in the last few months, including itself.

In March this year, Facebook announced it will buy Oculus VR, a California company specialising in virtual reality (VR) headsets, for around $2bn. Apple's acquisition of Beats Electronics for $3.2bn is its biggest ever expenditure on a takeover. Beats is not huge: it has 27% of the $1.8bn US headphones-business, mainly because of its premium pricing, but it has 57% of that market's premium sector and a music streaming service, both of which can nicely bolster Apple's existing offerings in wearable electronics.

Facebook and Apple do not talk of paybacks, calling their investments strategic. Many of these huge "gut-feel" investments also tick a box under new, hot topics that overlap with wearable technology, such as the Internet of People (IoP) or the Internet of Things (IoT). Market specialist IDTechEx predicts that as many as 55 billion IoP devices will be in use in 2025, many employing printed, flexible electronics and completely new components.

Recently, Google paid a strategic $3.2bn for the small IoT/IoP company called Nest Labs that has made a few million connected smart thermostats and smoke and carbon-dioxide detectors, which can respond to users' needs much like wearable technology.

On the other hand, it's been reported that Google has already committed at least $1bn on the development of Google Glass, on an experimental diagnostic contact lens for diabetics and on a planned smart watch; all three fall into the IoP category.

All of these devices are not just applicable to the consumer and medical markets; many will have wider uses, and especially in industry. In February 2014, GE announced it would invest $1.5bn into "industrial Internet" research from 2012 to 2015. Cisco, with over $46bn in the bank and intense interest in IoP and IoT, probably has its ears pricked up, hoping for an early participation in these markets as a system integrator. Microsoft, IBM and Oracle are also circling. The investment frenzy continues.

FactSet has named the top ten cash-rich companies, and half of them are in the tech industry: Microsoft, Google, Cisco, Apple and Oracle. Combined, these five tech companies hold $245bn in cash and all are intensely interested in wearable technology, IoT and IoP. Sprinkling a few billion here and there to participate is not going to break the bank for any of them, so now is a good time to be a small business launching inspired wearable and other consumer or medical electronics technology. Smaller companies might even hope to get bought for an eye-watering sum if their developments happen to be smack in the middle of these interests.

In addition to IoP, there's also the smaller but still substantial sector of wearable electronics for animals, with an initially addressable market of 20 billion units. The big boys might be giving that a miss for now, but soon that business will add substantial wearable electronic ID, diagnostics, location and treatment of endangered species as we destroy the world around us.

By Dr Peter Harrop from IDTechEx, which offers the following reports linking to the wearable electronics markets: "Wearable Technology 2014-2024: Technologies, Markets, Forecasts", "E-Textiles: Electronic Textiles 2014-2024", "Internet of Things (IoT): Business Opportunities 2015-2025" and "Internet of People: Technology 2015-2025". For more information, see www.IDTechEx.com/Research.

EDITOR: Svetlana Josifovska
Tel: +44 (0)1732 883392
Email: svetlanaj@sjpbusinessmedia.com

SALES: John Steward
Tel: +44 (0)20 7933 8974
Email: johns@sjpbusinessmedia.com

DESIGN: Tania King
PUBLISHER: Wayne Darroch

ISSN: 1365-4675

PRINTER: Buxton Press Ltd

SUBSCRIPTIONS:
Subscription rates:
1 year: £59 (UK);
£85 (worldwide)
Tel/Fax +44 (0)1635 879361/868594
Email: electronicsworld@circdata.com

SJP business media

Follow us on Twitter @electrowo

Join us on LinkedIn

NEW GRAPHENE-TYPE MATERIAL CREATED

Scientists at the University of Liverpool have created a new material related to graphene that has the potential to improve transistors used in electronic devices.

The new material triazine-based graphitic carbon nitride (TGCN) was theoretically predicted in 1996, but this is the first time it has been made.

Graphene is one atom thick, strong and conducts heat and electricity highly efficiently. The new TGCN material is also two-dimensional, but it has an electronic band-gap, making it potentially suitable for use in transistors.

At present, transistors are made of expensive silicon that generates heat when used in electronic devices. Scientists have been looking for a material that is carbon-based and has the electronic band-gap needed for use as a semiconductor.

"This is an exciting result because there are relatively few ordered two-dimensional organic solids. Finding a new member of the graphene family is very significant," said Professor Andrew Cooper, from the University's Department of Chemistry.

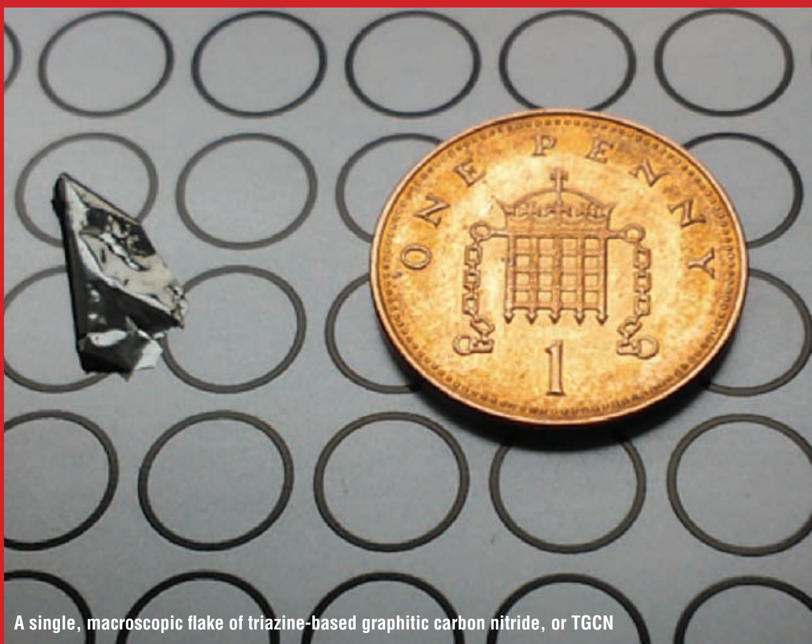

A single, macroscopic flake of triazine-based graphitic carbon nitride, or TGCN

Starting with the inexpensive molecule dicyandiamide, the team prepared crystals of graphitic carbon nitride, a two-dimensional layered material that is similar to graphene, but which contains nitrogen. They combined the ingredients in a quartz tube and heated them for 62 hours at up to 600°C. The result is a liquid containing flakes of TGCN that can be removed by filtering or peeling them off the quartz tube.

The material is at an early stage of development and Professor Cooper believes the next stage in the research is to explore its properties.

"The creation and analysis of this material is just the first step. We now have a lot more work to do to scale it up and prove its function in electronic devices," said Cooper.

The research project, funded by an Engineering and Physical Sciences Research Council (EPSRC) Programme grant at Liverpool, also involved chemistry, physics and materials science researchers from across Europe. This team included scientists at Technical University Berlin, Ulm University, Aalto University, Humboldt University Berlin, University College London, University of East Anglia, University of Helsinki, and the Max Planck Institute for Colloids and Interfaces.

ZHAGA AIMS TO ENABLE INDEPENDENT INTERCHANGEABILITY OF LED MODULES AND DRIVERS

The Zhaga Consortium plans to enable LED modules and drivers to be independently interchangeable. This is in addition to Zhaga's aim to enable interchangeability of LED light engines.

At present, the Zhaga interface specifications (known as Books) define interchangeable LED light engines (LLEs) that may have an integrated driver, or may consist of a driver that is separated from one or more LED modules. Currently, Zhaga Books exclude the electrical interface between the module and the driver. The consequence is that, for LLEs having a separate driver, it may not be possible to interchange LED modules from different suppliers without also using a different driver, or vice versa.

With this decision, the Zhaga Consortium is responding to the market need for LED modules and LED drivers that are independently interchangeable. To achieve this independent interchangeability, future editions of Zhaga Books may need to include references to specifications that define the module-driver electrical interface.

In the four years since Zhaga was formed, technical solutions have emerged that make it possible to define module-driver interfaces for specific application segments without limiting innovation in LED module and driver technology.

"The Zhaga Consortium believes that now is the right time to develop specifications for the module-driver interface and enable independent interchangeability of LED modules and LED drivers," said Musa Unmehopa, who replaced Menno Treffers as Secretary General of the Zhaga Consortium on April 1, 2014.

Zhaga is identifying other organizations that are also interested in developing driver-module interface specifications. Zhaga's aim is for these interfaces to be defined quickly and without unnecessary duplication of efforts in the lighting industry.

TURNING LEAD TIMES INTO TRANSIT TIMES:

How Digi-Key's Unique In-Stock Model is Effectively Eliminating Lead Times and Turning Electronic Component Distribution on its Head

Product lead times. A seemingly necessary evil in the ever-changing component distribution market. Historically, these lead times have been relegated as part of the design process, a factor that requires a definite plan at the outset of product design. As an example, let's start with a hypothetical situation.

Dawn is an enterprising engineer with a passion for gardening. However, this passion does not extend to the wildlife currently wreaking havoc on her newly budded berry bushes. Putting on her thinking cap, she sits down in her home office and devises a rather clever Arduino-based system to solve her quarrel with Mother Nature. The system would attack the problem on multiple fronts, measuring soil moisture and providing water to her plants accordingly, while controlling a system of motion-activated water jets to scare away deer, birds, and other marauding pests.

Excited to build her new project, she seeks out the parts she needs to complete the project from several online sources. Much to her dismay, every option for sourcing the one particularly specialized part that she needs currently has at least a twelve-week leadtime, well past the period in which she will be able to save her beleaguered berries.

Though slightly fantastical and a bit over the top, the tale above highlights the reality of a widespread occurrence within the engineering community. Whether due to the obscurity of the part, the volume of product needed, or other extenuating factors, designers, purchasers, and companies are often faced with the challenge of sourcing the parts they need on less than ideal timelines.

Market uncertainties affect lead times

Rising fuel costs leading to further use of slower, more economical modes of transport; global outsourcing of manufacturing; as well as a resistance toward maintaining high levels of stock are all factors leading to increased lead times. Market volatility and related customer demand fluctuations have led many companies to operate on much tighter stock levels, resulting in an associated rise in lead times.

Digi-Key, however, has devised a fairly simple, yet elegant, solution to the issue of lead times: maintain the industry's largest breadth of in-stock product, available for immediate shipment.

Whether by being one of the first distributors to break down standard package sizes, by being one of the earliest adopters of the e-commerce model, or by eschewing traditional methodologies regarding the depth of in-stock product, the company has a rich history of innovation.

From the company's earliest days, Digi-Key has blazed its own trail, valuing pursuit of the highest level of service and finding new and exciting ways to provide the best research and buying experience possible to its customers. After much reflection and deliberation, it was decided that first and foremost in achieving these goals was getting product into the hands of engineers quickly, efficiently, and accurately. This led the company to move past traditional ideologies regarding stock levels and take a radical approach.

One million factors in reducing lead times

Digi-Key stocks one million individual SKUs. Not offers. Not makes available at a later date. *Stocks.*

Each and every stocked product is available for immediate shipment, anywhere in the world. No other distributor offers this breadth of in-stock product, a designation very close to the heart of Digi-Key. The company's value proposition of providing the broadest selection of in-stock products available for immediate shipment hinges on maintaining this extraordinary level of product at all times. An extensive team of Digi-Key staff works tirelessly to liaise with suppliers and carriers to ensure that when a customer clicks 'Buy Now' on the Digi-Key website that the product is on the shelf, ready to be picked, packed, and shipped out across the globe, often out the door in a matter of minutes.

This speed of service has broken down many of the misconceptions about the cons of doing business with a company outside of the customer's home country. As customers realize that Digi-Key has removed many of the geographical barriers and hindrances to ordering internationally, there is a significant change in mindset pushing customers toward caring more about getting the products they need, when they need them, and less about where the products originate. The company's status as an authorized distributor of each product they carry assures customers they are receiving quality product direct from the manufacturer.

However, the greatest benefit can be found when looking at Digi-Key's "lead times". Depending on where the product is being sent and which of the myriad shipping methods is chosen, customers can have their product in their hands the next day. The company's customer-focused stock maintenance plan has all but eliminated lead times for the one million products they keep on the shelf.

Through extensive market research and planning, Digi-Key is able to take on and effectively shield customers from any existing lead times, mitigating carrying cost and wait time for customers. By effectively removing lead times from the equation, customers are able to get the components they need on their time schedule, in their preferred quantity, streamlining the design process and helping to accelerate how quickly end products can hit the market.

As more and more customers have come to rely on Digi-Key for their prototype quantity product needs, they have found that the company's model offers a seamless transition into production-level sourcing of product. An increasing number of production-level customers around the world turn to Digi-Key for access to the widest BOM coverage in the industry supported by a full suite of supply chain services. Companies can run faster and leaner by leveraging Digi-Key's ability to reduce or even eliminate carrying costs associated with the sourcing process.

"Overall, the success of the Digi-Key model is built upon the promise of supporting the needs of the design engineer, a segment we understand intimately over 40 years in the business," said Dave Doherty, Digi-Key Executive Vice President of Operations. "Today, we've scaled our business to support a broader range of global customers representing businesses of all sizes."

As Digi-Key continues to evolve in response to changing customer expectations and needs, the company will remain fully committed to offering the broadest selection of in-stock product in the industry, coupled with a robust offering of technical resources and tools. Customers will continue to be able to count on Digi-Key to have the parts they need, when they need them, supporting the product design process from Prototype to Production®.

Ian Wallace
Ian.wallace@digikey.com
Tel: +44 (0) 1344 204022
www.digikey.co.uk

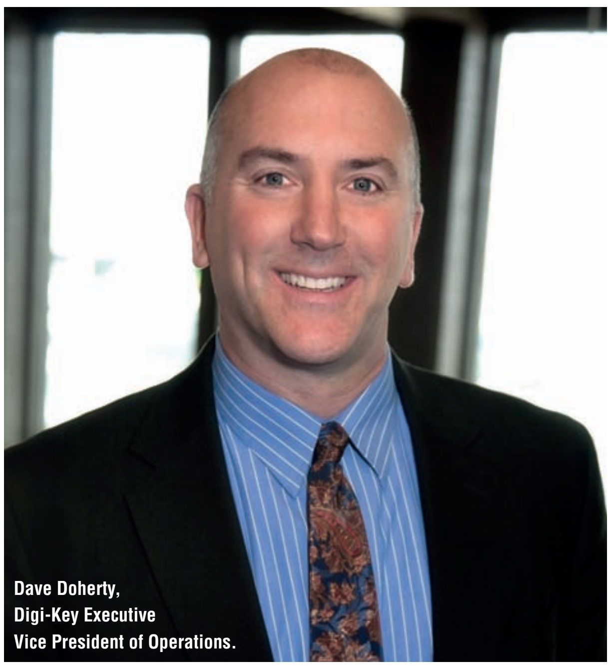

**Dave Doherty,
Digi-Key Executive
Vice President of Operations.**

Two Aerials?

MYK DORMER IS A SENIOR RF DESIGN ENGINEER AT RADIOMETRIX LTD **WWW.RADIOMETRIX.COM**

When a piece of radio equipment (often a Wi-Fi hub or repeater) is seen sporting a pair of identical looking antennas, radio engineers will often sagely nod their heads and mutter something approving about this being the mark of a "diversity radio system".

All very well, but what does "diversity" mean in such a context?

Diversity operation is actually a general term referring to any radio system which uses two or more communication channels to increase the reliability of the link. This could be multiple frequencies (discrete channel or spread spectrum), multiple transmission bursts or "time diversity" (best suited to protect against discrete bursts of interference) or spatial diversity, where several different propagation paths are used to alleviate the effects of fading (phase cancelation related signal nulls). This technique, also referred to as "antenna diversity" is the one associated with the commonly seen multiple antennae, and is a technique that can be usefully applied to simple ISM band low-power radio systems without a great deal of complication.

> "Applying diversity to a low-power wireless application is (relatively) simple, and can yield considerable benefits in terms of range and reliability

Antenna diversity is not, in itself, an especially new technique. It was first prototyped in the early 1920s by Beverage and Peterson, and was in commercial radio-telegraph use by RCA by the end of the decade. The value of the method is that it provides a way to overcome the fading effects that occur when there are multiple signal paths (for example a direct path and a reflection from a nearby building) between transmit and receive locations, and the multiple incident signals arrive out of phase and cause destructive cancelation or "nulling". These nulls can reduce signal strength by 20dB or more, and can be constant, or variable (with the movement of reflecting surfaces on vehicles, or changes in atmospheric conditions).

Antenna diversity is a solution for this as it provides two or more antennae at either the transmit or receive ends of a link, separated by a half wavelength or more, resulting in a situation where, if one antenna is in a deep fade, it is unlikely the other will be, too. Add more antennas and the probabilities become increasingly favourable.

Applying diversity to a low-power wireless application is (relatively) simple, and can yield considerable benefits in terms of range and reliability. In the simplest case, it comes down to a choice of transmit- or receive-end diversity, with each having its own benefits and tradeoffs:

- A basic transmitter diversity system has a pair of antennae at the transmitting end and sends a consecutive pair of identical transmissions, one through each antenna, using either an RF switch or separate transmit circuits. This imposes a cost in terms of channel capacity (at least halving data throughput), but actually provides both time and spatial diversity, minimizing burst and fading effects, and the simple receiver-end system need only be able to handle the multiple copies of the sent data burst.
- The simplest way to implement receive diversity in an ISM-band link is to duplicate the whole receive path, from antenna through receiver to the decoder, and then select whichever decoder output is error-free. This imposes an increase in hardware cost and size, but requires only a single transmit burst (so is more spectrally efficient) and has a minimal (or zero) processing overhead. Noise-correlation effects may also provide an overall improvement in receive sensitivity, a technique that can sometimes be added to an existing system without significant modifications to the rest of the hardware or system architecture.

Diversity is not suited to every system (issues of throughput, power consumption, size and cost will frequently intervene), but where the absolute longest possible range for the given power level and data rate is needed, and the antenna location cannot be improved any further, then it might just be the technique to reach out that vital extra distance. ●

HOW TO ELIMINATE MECHANICAL SWITCHES FROM THE USER INTERFACE

BY **DAVID POTT**, DIVISIONAL MARKETING MANAGER AT ANGLIA COMPONENTS LTD

The user interface of most electronic systems is still dominated by mechanical switches, ignoring the development, in recent years, of reliable touch-control technologies like metal over capacitive switches. These technologies eliminate the need to cut an aperture, enhancing the styling of the system, and fully overcome the traditional limitations of capacitive touch switches.

Advantages

One of the greatest advantages of a metal over cap touch control switch system is the flexibility of its sensors. The switch can be fully integrated with the front panel. Hundreds of different sensor designs are possible, and the same look and feel can be achieved using several different implementations. It is possible to backlight by selectively perforating the metal plate, or add braille lettering. A plastic look and feel can be created using a metal film (see Figure 1c) or various different types of metal, and it is even possible to use metalized rubber if that is the desired effect. The facia can be produced in various types of metal, with a textured finish if required (see Figure 2), which is not only attractive, but can also increase the deflection of the facia so a thicker metal can be used.

> “Metal over cap controls share all the virtues of capacitive touch buttons: low power, low cost and reliable mechanically, but also overcome the traditional limitations without compromising power consumption or design simplicity

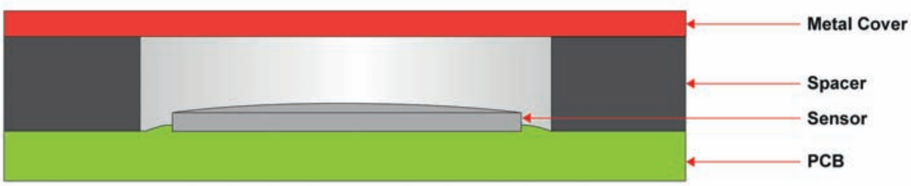

Figure 1a: Cross-section of metal over capacitive (unpressed) switch

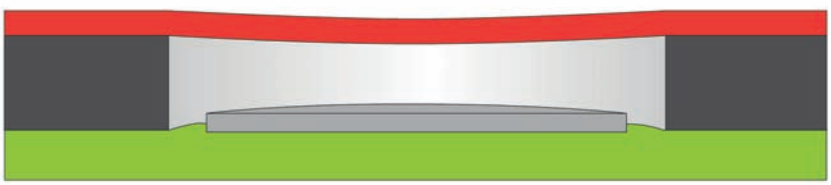

Figure 1b: Cross-section of metal over capacitive (pressed) switch

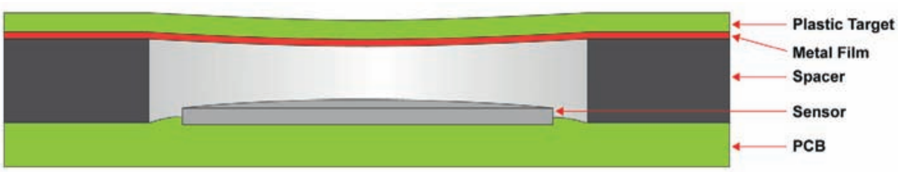

Figure 1c: Cross-section of metal over capacitive (pressed) switch using a plastic target

Metal over cap controls share all the virtues of capacitive touch buttons: low power, low cost and reliable mechanically, but also overcome the traditional limitations without compromising power consumption or design simplicity. Unlike standard touch systems, this technology will work through metal, isn't affected by gloved hands, and doesn't normally require special software to handle electrically noisy environments. There is also no issue with reading buttons in the presence of water or other contaminants.

Designing A Touch Control

There are two aspects to designing a touch control solution – the mechanical and the electronic design. Both are extremely straightforward, and component manufacturers provide design tools and other support to simplify the process further.

In terms of mechanical design, the main issue is ensuring that the right spacing is specified. The tools available will model

Figure 2: Textured metal coatings

Figure 3: Microchip's deflection tool

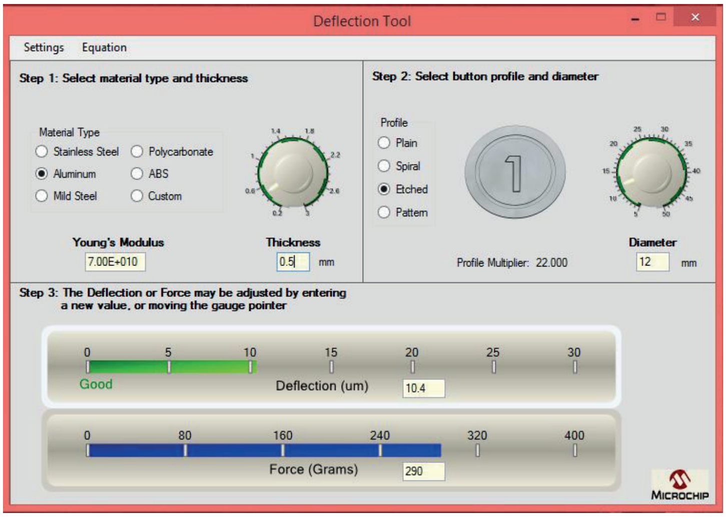

the expected response of the button, given various mechanical parameters (see Figure 3).

In electronic terms, the best ways of measuring the capacitance of the switch to detect a touch are a differential capacitive voltage divider (CVD) and a charge time management unit (CTMU).

The CVD acquisition technique can be implemented in most microcontrollers, including Microchip PICs, and requires an Analog-to-Digital Converter (ADC), a pin per button and a minimum of digital processing overhead. However, for microcontrollers that don't have a large enough sample-and-hold capacitor on their ADC to produce an accurate CVD solution, the CTMU approach is available.

Differential Capacitive Voltage Divider

Capacitive sensors are most commonly created by placing an area of metal-fill on a printed circuit board. This conductive pad is then connected to a microcontroller device through a thin trace and an optional series resistor. The microcontroller will continuously poll the capacitance of the pad and watch for a significant shift to occur. The definition of "significant" depends on the level of noise, however. The shift must be appreciably higher than the noise level in worst-case conditions.

Charge Time Management Unit – CTMU

Some microprocessors have an on-board peripheral feature called a Charge Time Management, which is a constant-current source, surrounded by digital circuitry to precisely control its operation. The current source operates over four decade ranges, from 0.55µA to 550µA. When combined with the on-chip A/D converter and comparators, the CTMU can perform capacitive measurements, both relative and absolute.

Dedicated Cap Touch Buttons

There are also dedicated capacitive touch sense devices available, implementing between one and 14 buttons. These devices, controlled by I2C or SMBus, are straightforward to set up, and offer the option to program the sensitivity. They can also automatically compensate for gradual changes in environment.

Getting To Market

There is a little more electronic and mechanical design effort involved in implementing a touch control but this is a small price to pay for the many advantages. Eliminating apertures from the enclosure can reduce its cost and make it much easier to seal against the environment. Eliminating switches can enhance reliability and reduce maintenance. These two considerations alone should make the economics of touch control attractive.

The most compelling argument, though, is probably appearance. Professional as well as consumer electronics need to 'sell' themselves to the user, and a well-designed enclosure is now a must. The enclosure normally needs to be designed around the mechanical switch array. With touch controls, the flexibility is so great that they can essentially be designed into the desired enclosure. ●

OPERATING PRINCIPLE OF METAL OVER CAP

In a traditional capacitive system, the user changes the capacitance of a touch sensor by placing their finger in close proximity to the sensor. The user's finger then forms the second plate of a capacitor, raising the sensor's capacitance.

The metal over cap touch system uses a conductive layer, suspended over the capacitive touch sensors, to form the second plate of the capacitor. When a user applies a downward pressure on the conductive layer, the resulting deformation moves it closer to the capacitive sensor. The change in spacing produces a change in capacitance, which is then measured by a microcontroller.

See Figure 1a for a cross-section of a typical metal over capacitive touch sensor; Figure 1b demonstrates the deformation due to a user's press; and Figure 1c shows an alternate configuration where the target can be either a thin sheet of metal bonded to the back of the plastic fascia, or a metal flashing onto the plastic sheet.

REED RELAY BASICS

BY **KEVIN MALLETT**, PRODUCT MANAGER FOR REED RELAYS AT PICKERING ELECTRONICS LTD

In principle, reed relays are deceptively simple devices (see Figure 1). They contain a reed switch, a coil for creating a magnetic field, an optional diode for handling back EMF from the coil, and a method of connecting the reed switch and coil to the outside of the packaging.

The reed switch has two, shaped, metal blades made of a ferromagnetic material (roughly 50:50 nickel iron) and glass envelope that holds the metal blades in place and provides a hermetic seal preventing any contaminant entering the critical contact areas inside the glass envelope (see Figure 2).

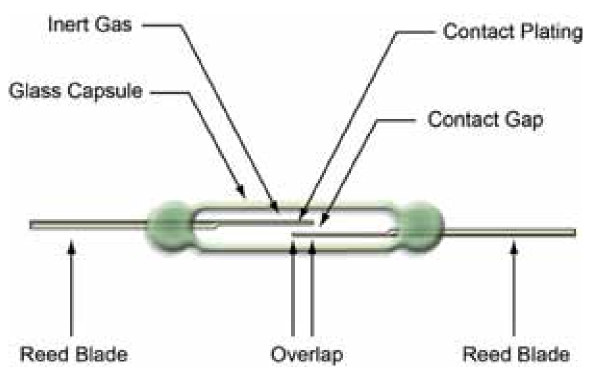

Figure 1: Reed relay diagram

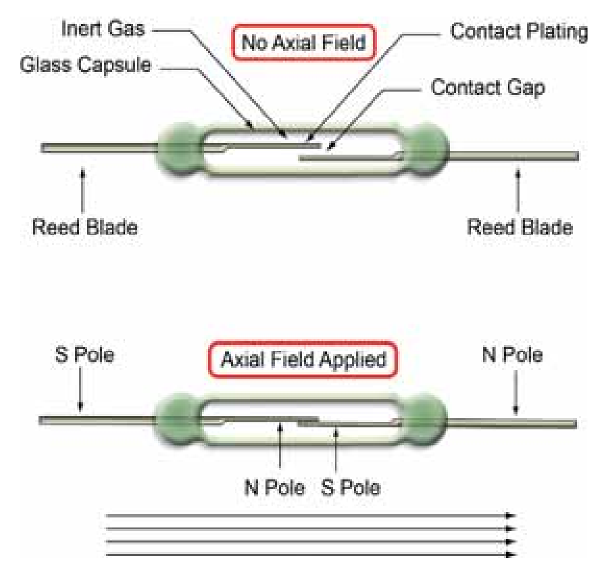

Figure 2: Reed switch

Reed Relay Characteristics

In their normal state, most (but not all) reed switches have open contacts. When a magnetic field is applied along the axis of the reed blades, because of their ferromagnetic nature the field in them intensifies, pulling them together until closing the contacts and establishing an electrical contact (see Figure 3).

The deflection of the blades is the only movable part in the reed switch, which means effectively there are no mechanical parts that can wear out. Since the contact area is enclosed in a hermetically-sealed envelope, this gives the reed switch an exceptionally long mechanical life too.

Inevitably, the issues are a little more complicated in practice. The ferromagnetic material is not a good conductor and, in particular, the material does not make a good switch contact. So the reed blades need a precious metal cover in the contact area, and to ensure good adherence there is also an underlying metal barrier.

Some types of reed relays use mercury wetted contacts, consequently reed relays with plated contacts are often referred to as "dry" reed relays. The metals can be added by selective plating or by sputtering processes. Where the reed blade passes through the glass envelope, any plating (in many cases there may be none) requires careful control to avoid damaging the hermetic seal. Outside the glass seal, the reed blades have to be suitably finished to allow them to be soldered or welded into the reed relay package, usually requiring a different plating finish from that used inside the glass envelope.

The materials used for the contact areas inside the glass envelope have a significant impact on the reed switch (and therefore the relay) characteristics. Some materials have excellent contact resistance stability; others resist the mechanical erosion that occurs during hot switching events.

The material for the contact is chosen to best suit the target performance, especially considering its significant impact on the manufacturing cost. Commonly-used materials are ruthenium, rhodium and iridium – all of which are in the relatively rare platinum precious metal group. Tungsten is often used for high-power or high-voltage reed switches due to its high melting point.

Another design variable of the reed switch is its size. Longer switches do not have to deflect the blades as far (measured by

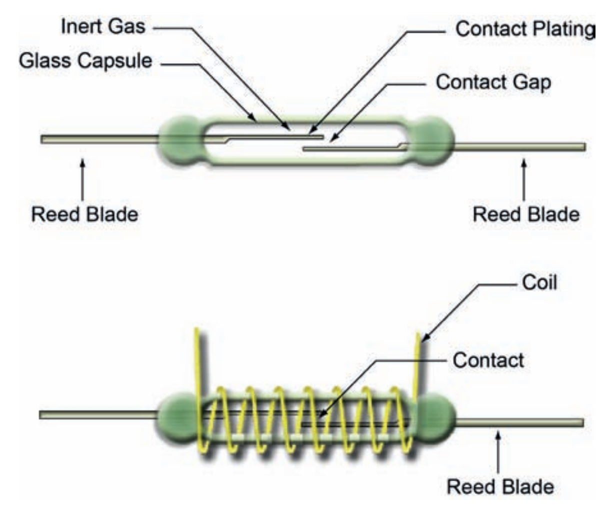

Figure 3: Generating a magnetic field

angle of deflection), as short switches to close the gap between the blades. Short reeds are often made of thinner materials so they deflect more easily, but this clearly has an impact on their rating and contact area. Smaller reed switches allow smaller relays to be constructed – an important consideration where space is critical, whereas the larger switches may be more mechanically robust and have greater contact area, improving their signal carrying capability.

It is these compromises in reed switch design that gives rise to the sometimes bewildering range of reed relays that are available with both subtle and dramatic differences in performance.

Generating The Magnetic Field

For a relay, a magnetic field needs to be created that is capable of closing the reed switch contacts. Reed switches can be used with permanent magnets, for example to detect closing doors, but for the reed relays described in this article the field is generated by

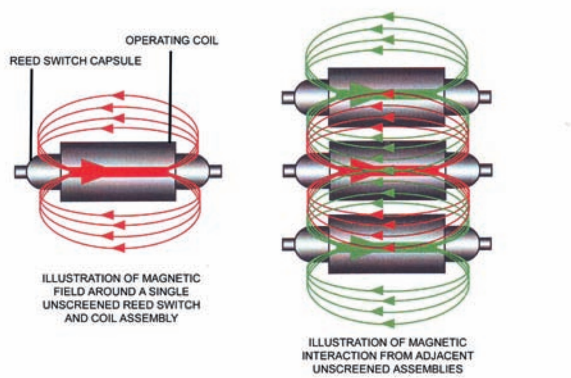

Figure 4: Magnetic interaction

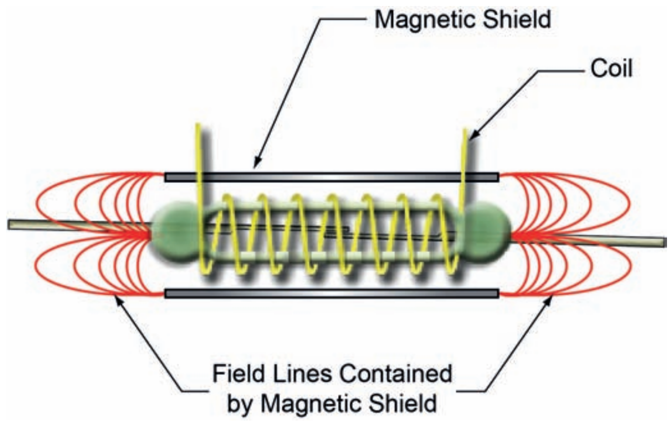

Figure 5: Shielded relay

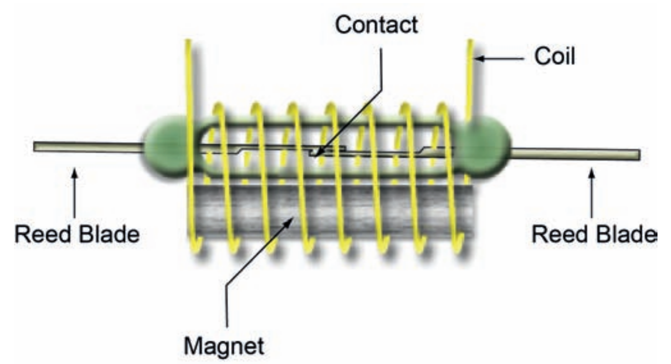

Figure 6: A normally-closed reed relay

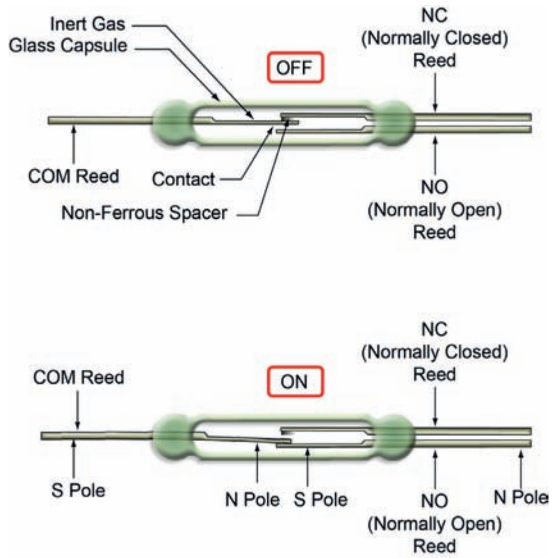

Figure 7: Changeover reed switch

a coil with current passing through it in response to a control signal. The coil surrounds the reed switch and generates the axial magnetic field needed to close the reed contacts.

Different reed switches require different levels of magnetic field to close the contact, and this is usually quoted in terms of ampere turns (AT), which is simply the product of the current flowing in the coil multiplied by the number of turns. Again, this creates a great deal of variation in reed relay characteristics. Stiffer reed switches for higher power levels, or high voltage switches with larger contact gaps, usually require higher AT numbers to operate, so the coils require more power.

Use of different wire gauges for the coil and number of turns creates relays with different drive voltage requirements and different coil powers. The resistance of the wire coil controls the amount of steady-state current flowing through the coil and therefore the power the coil consumes when the contacts are closed. Whenever fine wires are used in Pickering relays, the termination leads from the coils are skeined with several strands of wire twisted together to increase their physical strength. Larger coils can be used to reduce power consumption, but that increases the size of the relay.

A significant factor in some designs is the ability to drive reed relays with standard CMOS logic, requiring the coil to operate from 5V or 3.3V and that the current (power) requirements in coil are minimized.

Protection Against Magnetic Fields

The fact that reed relays are magnetically operated causes a potential problem for users when they are assembled in dense patterns on PCBs.

The magnetic field required to close the reed blades flows through the nickel iron reed blades and returns by field lines which are outside the reed relay body. If several relays are close together, the external field lines include the neighbouring reed blades and either reinforce or partially cancel the field in the reed, changing the current needed to close or open the contact (see Figure 4). This can in some circumstances cause the relay to either fail to close or to open, depending on the magnetic polarity. Some manufacturers suggest arranging the relays in different polarity patterns to mitigate the worst effect of the interaction, but this can become a complex compromise in dense arrays of relays where there are many near neighbours.

A much more sensible approach is to include a magnetic shield in the reed relay package (see Figure 5), an approach used by Pickering Electronics for many years. The user is then free to use a layout pattern that best suits the application. The approach has the added benefit of improving the coil efficiency since it concentrates the magnetic field lines closer to the reed switch body, shortening the magnetic field length outside the reed blades and creating a larger field for a given number of ampere turns in the coil. Lower coil-operating currents make coil driving simpler and improve other parameters like thermoelectric EMF generation.

Mercury Reed Relays

Historically, the class of reed relays where the electrical contact between the blades is enabled by mercury has been very popular. The mercury is provided by a small reservoir, and it is pumped up to the contact area (a grooved surface on the reed blade) by the blade's actuation, aided by mercury's high surface tension.

Selective chrome plating is often used in the construction since mercury and chrome do not stick together and this is used to help control the mercury.

The glass envelope of mercury relays is also highly pressurised (typically 12 to 14 bar), which helps manage the switch materials and operation and to improve electrical parameters. These relays are strongly preferred in some industries because they have a long contact life and bounce-free contact closure – a feature that is particularly helpful under hot-switch conditions. Stability of low contact resistance during their operational life is considered to be better than that of dry reed relays.

Most types of mercury reed relays are position sensitive – they can only be used in a vertical orientation. Some non-position-sensitive versions are also available, which can be used in any orientation. Mercury wetted relays however are not RoHS compliant and national regulations may limit their use in certain critical applications where exceptions to RoHS have been granted.

High Voltage Reed Relays

High-voltage reed relays, in addition to having to ensure high clearance distance (including the distance between the contacts in the reed switch), need an exact operating environment and different contact materials to resist the contact erosion that occurs when switching high voltages. High-voltage reed switches commonly use tungsten or rhodium contacts.

The glass envelope for high-voltage reed switches is normally a very hard vacuum to maximise the voltage rating for a given blade separation and to manage arc duration as the contacts open or close. Any loss of seal will rapidly degrade the switch operation, so reed switches have to be carefully managed during their assembly into reed relays.

Normally Closed Reeds

Most of the information in this article relates to normally open reed relays – by far the most common configuration. However, normally closed relays can also be supplied where the blade is biased to be normally closed and the application of a magnetic field opens the relay contacts (see Figure 6).

The contact bias is created by adding an internal permanent magnet to hold the reed switch in a normally closed state. When the relay coil is energised, the magnetic field bias is cancelled and the contacts open. If the coil voltage is increased substantially beyond its nominal voltage (typically greater than 1.5 times nominal) there is a risk that the contact will re-close.

Not surprisingly, normally-closed relays are more difficult to manufacture and have higher magnetic interaction due to the bias magnet.

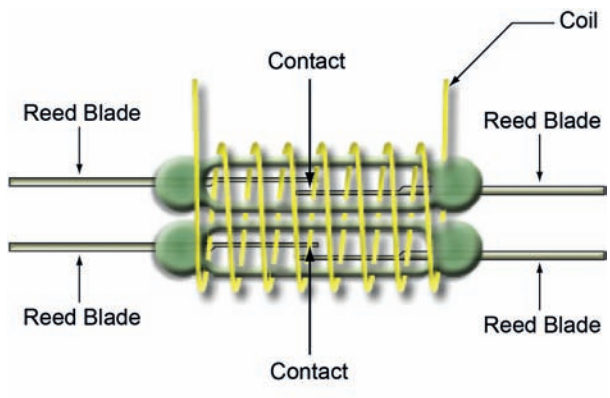

Figure 8: A two-pole relay

Changeover Reeds

Reed relays can be supplied with changeover switches (see Figure 7) – the reed switch has a normally-closed contact (when no magnetic field is applied) and a normally-open contact (which closes when the field is applied). The reed switch closed contact uses the blade as a spring bias with a non-ferrous spacer to avoid completing a magnetic circuit. The coil field moves the blade to the normally-open contact blade which does not have this spacer. As the reed relay switch blades transition between the two states for a brief period, neither contact is closed – an important consideration in some applications.

The normally-closed position relies on contact pressure being created by the spring bias of the blade. In addition to being much harder to manufacture than normally-open reed relays, the two contacts (normally closed and normally open) can have quite different characteristics and stability. Experience has shown that they have a slightly less stable contact resistance than their simpler normally-open counterparts. Even so, they perform a useful function for many applications because, unlike the use of two normally-open reed relays to create a changeover function, they only need one coil drive and it is mechanically not possible to have both contacts closed at the same time.

Two-Pole Relays

Reed relays can also be supplied as two-pole relays where two reed switches are contained in the same package and operated by a common coil drive (see Figure 8).

It is important to remember that these relays do not have an interlock mechanism between the two poles; it is unsafe to assume that that the two poles operate at exactly the same time; the two reed switches are essentially independent. There could be an operate time difference of betweeen 50-250µs between them. Failure in one (say a contact weld) will not stop the other contact from moving. ●

MAINTAINING INTERCONNECTIVITY IN THE HARSHEST ENVIRONMENTS

Dave Weaver at Bulgin discusses the benefits and some potential applications of the latest high power, waterproof push-pull power connectors.

Ensuring uninterrupted connectivity in the harshest environments is quite a challenge, requiring durable, environmentally-sealed connectors capable of withstanding even the most severe conditions. A variety of very successful metal and plastic connectors already exist, but there was a need to further extend the range to cater for applications using higher currents and larger cables. Building on the success of the Buccaneer® 6000 Series, Bulgin has developed a new range of larger diameter, higher power couplings; the Buccaneer 7000 Series of compact, environmentally-sealed 25A, 600V connectors.

Safe and secure connectivity

Water and dustproofing are important considerations when using electrical equipment. Besides the obvious hazard associated with water, salt water and dust, particularly cement dust, can erode contacts fairly rapidly, quickly rendering an unprotected connector useless. Traditional screw coupling waterproof connectors, while very effective, take time to couple. It can also be difficult to determine how tight the connections need to be to ensure they seal effectively. By contrast, the Buccaneer 7000 Series of compact and easy-to-use quick coupling connectors features a unique tri-start thread, twist locking system with positive feedback; ideal for 'blind' or awkward mating situations. This enables a water and dustproof seal to be made quickly and easily in less than a quarter of a turn without the need for technical expertise, reducing the potential for operator error.

An extensive range of applications

Connectors play an essential role in an incredibly diverse range of applications. With interest in renewable energy continually growing, one potential application for easy-to-assemble, 'fit and forget' connectors is solar technology. Solar inverters are connected to solar panels via single pole connectors, and high power output connectors are required to carry the mains voltage back to the grid. The Buccaneer 7000 Series is ideally suited to this application, offering safe, secure connection in a compact unit capable of withstanding long-term outdoor exposure.

Robustness is vital for industrial automation purposes – where constant power distribution and process control are essential – as well as for large weighing equipment and transportation applications, such as the specialist vehicles used to inspect rail tracks. Connectors used for these applications must withstand considerable stress, and durability is a prerequisite to avoid unplanned downtime. Rugged, rapid-locking connectors with positive feedback achieve a perfect 'fit and forget' seal every time, without the need for technical expertise or specialist tools.

For many applications, waterproof connectors are a key requirement. Temporary lighting and sound systems at concert venues rely on durable, waterproof connectors capable of accommodating large cables to provide a secure, stable power supply. These connectors are also ideal for water features such as fountains, offering a secure mains interface for pumps and underwater lighting. For marine applications – typically winches and lighting equipment – connectors must be both waterproof and resistant to salt water corrosion, and the use of plastic, rather than metal, connectors can be beneficial.

A rugged and versatile solution

Designed to withstand the harshest conditions, the durable Buccaneer 7000 Series connectors have a single piece body and meet IP66, IP68 and IP69K standards, making them suitable for a diverse range of different applications and environments, as well as allowing for changes in customer specifications. With body mouldings and pin carriers designed to create a robust interface while preventing damage during coupling, a correctly sealed connection is guaranteed even where access is restricted, giving engineers and product design professionals increased flexibility for a broad range of applications.

Interchangeable plastic and metal connectors are available, enabling an extensive range of different applications to be accommodated. Light weight, versatile and cost-effective plastic couplings are less prone to the risk of moisture accumulating within the connector and more resistant to attack by salt water, as well as UV-stable, making them ideal for long-term use in outdoor applications. In addition, these UL94 V-0 rated self-extinguishing connectors are halogen-free, ensuring that, in the event of fire, no toxic gases are emitted.

Where a more robust and rugged material or electromagnetic compatibility are required, metal connectors are more suitable, providing continuation of the cable screen from the cable through to the mating connector and completing the Faraday cage. For maximum flexibility, metal and plastic can be interchanged. Customers needing protection from electromagnetic interference may choose to combine a metal connector with the corresponding plastic mating connector, reducing the cost as much as possible. Equally, for some applications a plastic connector may be the ideal solution, yet the cable mounting half of this interface may need the additional strength of a robust metal connector to ensure it is not damaged in use.

Conclusions

In any industry, reliability is a crucial consideration, since failure of a single connection may result in a lengthy period of downtime and significant revenue losses while the fault is diagnosed. The larger diameter, higher power Buccaneer 7000 Series connectors enable a water and dustproof seal to be made quickly and easily, allowing rapid installation, replacement and maintenance of equipment without the need for specialist tools or expertise. With rigorous IP66, IP68 and IP69K rated ingress protection, the connectors are suitable for almost any application. This provides customers with total confidence in the quality and reliability of their chosen products, which have been developed using tried and trusted design techniques and knowledge acquired over many years to guarantee trouble free, ‘fit and forget’ connectivity in the harshest of environments.

For more information about Bulgin products,
please contact:
Elektron Technology, Woodland Road,
Torquay, Devon, UK TQ2 7AY
Tel: +44 (0)1803 407700
connectivity@elektron-technology.com
www.bulgin.co.uk

HIGH-FREQUENCY MODEL OF ELECTRIC VEHICLE LI-ION BATTERY

MO YAO, YONGMING YANG AND **QUANDI WANG** FROM CHONGQING UNIVERSITY IN CHINA DESCRIBE THE HIGH-FREQUENCY IMPEDANCE CHARACTERISTICS OF A LI-ION BATTERY USED IN ELECTRIC VEHICLES, AND SUGGEST HIGH-FREQUENCY MODELS OF A SINGLE AND MULTIPLE BATTERY CELLS CONNECTED IN SERIES, PROVIDING BASIS FOR THE ANALYSIS OF ELECTROMAGNETIC INTERFERENCE, WHERE THE BATTERY ACTS AS A PROPAGATION PATH

Batteries are widely used in portable electronic devices and, recently, the design of very advanced rechargeable batteries for electric vehicles has attracted the attention of many researchers. Battery research focus varies, from the power interface, state-of-charge estimation, state-of-health and cycle-life prediction to the battery's application limitations. Many projects also focus on the cycling and static characteristics of the battery, including its frequency characteristics.

The Li-ion battery tends to be the primary power source in electric vehicles, typically connected via a DC/AC converter to the motor drive. However, its high-power switching generates high-frequency harmonics that tend to propagate through the system, resulting in electromagnetic interference. As such, establishing a high-frequency model of the battery is an important step toward identifying and eliminating that interference.

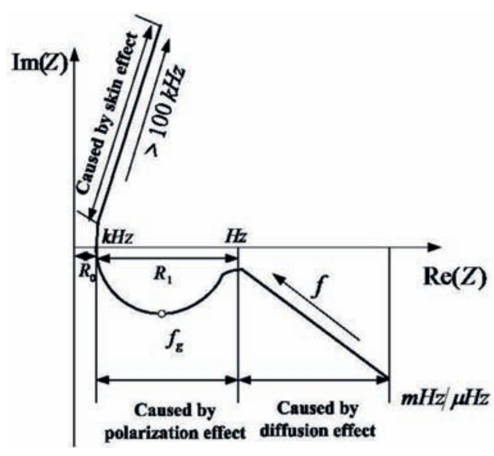

Figure 1: Nyquist plot for a battery's frequency characteristics

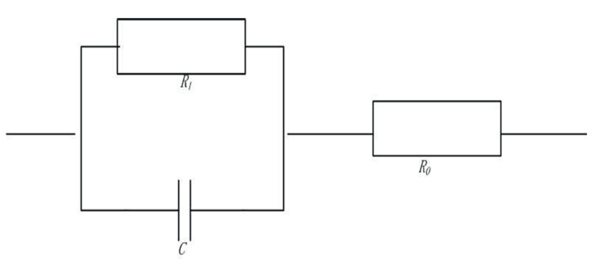

Figure 2: Impedance equivalent circuit of a battery under polarization

Factors Affecting Battery Impedance

Several conditions affect electric vehicle operation, including the vehicle's battery charge-discharge cycle, battery aging, cycling current, state of charge (SOC) and so on.

The impedance of a battery is typically affected by the system's operation as well as the battery's structure and chemistry, factors which can lead to varied battery responses to AC signals, and effects known as diffusion, polarization and skin effect, among others.

The frequency characteristics of the system can be shown simply by a Nyquist plot (see Figure 1), in this case depicting the battery's diffusion effect, polarization effect and skin effect. A Nyquist plot can simultaneously show real as well as imaginary frequency, amplitude-frequency and phase-frequency characteristics.

The frequency of the AC signal can impact a Li-ion battery, causing diffusion and migration of ions in its solution, affecting its impedance. In the Nyquist plot, this is shown as a line at a 45-degree angle.

When the frequency of the AC signal rises, the influence of ion diffusion on the battery's impedance decreases and the polarization effect takes over gradually. The equivalent impedance model of the battery under polarization is shown in Figure 2. It can be seen that when the frequency is above 1kHz, the polarization effect on the battery's impedance is very small, whereas the skin effect of the battery's electrodes and connecting wires make a big difference.

Measurement Setup

The complex impedance is measured in the frequency range 150kHz-30MHz with the Agilent impedance analyzer 4294A and its measurement fixture 16047E. The battery's electrodes cannot be connected to the fixture directly, as direct current

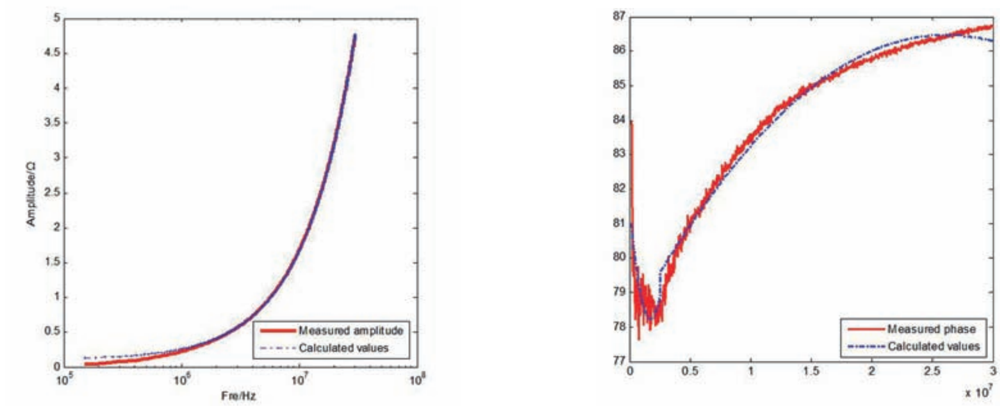

Figure 3: Figure 3: Comparison of the measured and calculated impedance curves for a cell: (a) amplitude-frequency; (b) phase-frequency

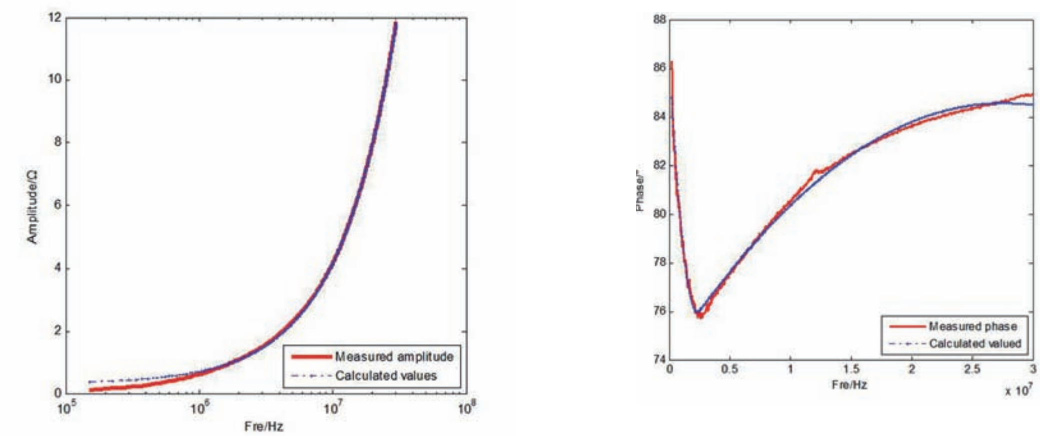

Figure 4: Comparison of the measured and calculated impedance curves for cells connected in series: (a) amplitude-frequency; (b) phase-frequency

will flow into the instrument and damage it, so a blocking capacitor (100uF) is used to prevent this.

The battery's anode is connected to one of capacitor's pins, with the other pin connected to the high port of the fixture. The fixture's low port is connected to the battery's cathode with as short a steel strip as possible. Likewise, the connecting wiring for the whole measurement system should be as short as possible to reduce the effects of wire impedance.

One other key requirement is that the capacitor breakdown voltage must be greater than the battery voltage to prevent breakdown; so, the larger the value of the block capacitor, the smaller its impedance will be.

The test signal used is 0.5V, sweeping between 150kHz-30MHz. Measurement results include battery impedance and block capacitor impedance under all conditions. However, for high-accuracy results, the impedance of the block capacitor must be removed from the total measurement result. The calculation of battery impedance is as follows:

$$Z_{total} = Z_{bat} + Z_{cap} = \mathrm{Re}(Z_{total}) + \mathrm{j}\,\mathrm{Im}(Z_{total}) \tag{1}$$

$$Z_{cap} = \mathrm{Re}\ Z_{cap} + \mathrm{j}\,\mathrm{Im}(Z_{cap}) \tag{2}$$

$$\begin{aligned} Z_{bat} &= Z_{total} - Z_{cap} = \mathrm{Re}\ Z_{total} - \mathrm{Re}\ Z_{cap} + \mathrm{j}[\mathrm{Im}(Z_{total}) - \mathrm{Im}\ Z_{cap}] \\ &= \mathrm{Re}(Z_{bat}) + j[\mathrm{Im}(Z_{bat})] \end{aligned} \tag{3}$$

where Equation 1 is the total impedance, including battery and capacitance impedances; Equation 2 represents the measurement of the capacitance impedance, and Equation 3 calculates the battery's impedance.

High-Frequency Impedance Model

To build an EMC model for an electric vehicle, a high-frequency model for the batteries must be built first.

A polynomial equation based on the least square method is applied to create the mathematical model of the battery cell's impedance in the frequency domain. The *n*-order polynomial for the obtained data points $(x_i, y_i), 1 \le i \le N$ is:

$$f(x) = a_0 + a_1 x + a_2 x^2 + \circ \ = \sum_{k=0}^{n} a_k x^k \qquad (4)$$

To find the variation trend of the measured data points as accurately as possible we use curve fitting (a process of finding a best-match curve from a set of curves for a series of data points). Here, the errors between the fitting function value and the original value must be minimal:

$$|\delta_i| = |f(x_i) - y_i| \qquad (5)$$

Equation 6 is then:

$$\sum_{i=1}^{N} (\delta_i)^2 = \sum_{i=1}^{N} [f(x_i) - y_i]^2 = \min \qquad (6)$$

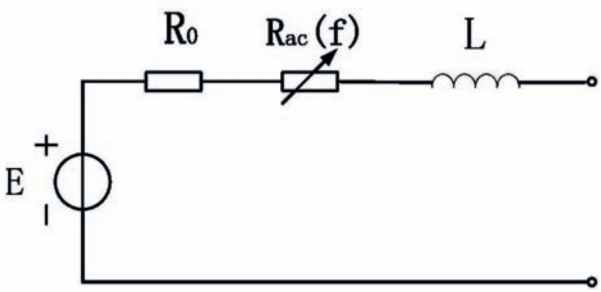

Figure 5: Impedance equivalent circuit of the battery with skin effect

To make Equation 7 achieve minimum value, the first order derivative of coefficients $a_k, 0 \le k \le n$ should be zero.

$$\frac{\partial S}{\partial a_k} = \sum_{i=1}^{N} 2k x_i^k [f(x_i) - y_i] = 0 \Rightarrow \sum_{i=1}^{N} x_i^k [f(x_i) - y_i] = 0 \Rightarrow \sum_{i=1}^{N} x_i^k f(x_i) = \sum_{i=1}^{N} x_i^k y_i \qquad (7)$$

where I = 1, 2,…, n. Equation 7 is simplified and rewritten as a matrix:

$$\begin{pmatrix} N & \sum_{i=1}^{N} x_i & \sum_{i=1}^{N} x_i^2 \\ \sum_{i=1}^{N} x_i & \sum_{i=1}^{N} x_i^2 & \sum_{i=1}^{N} x_i^3 \\ \sum_{i=1}^{N} x_i^2 & \sum_{i=1}^{N} x_i^3 & \sum_{i=1}^{N} x_i^4 \end{pmatrix} \cdot \begin{pmatrix} a_0 \\ a_1 \\ a_2 \end{pmatrix} = \begin{pmatrix} \sum_{i=1}^{N} y_i \\ \sum_{i=1}^{N} x_i y_i \\ \sum_{i=1}^{N} x_i^2 y_i \end{pmatrix} \Rightarrow y = a_0 + a_1 x + a_2 x^2 \qquad (8)$$

The amplitude-frequency characteristic function is calculated in Equation 9:

$$Z_0(f) = 1.56 \times 10^{-7} f + 0.1054 \qquad (9)$$

The phase-frequency characteristic function is determined by Equation 10:

$$\theta = \begin{cases} 1.06 \times 10^{-12} f^2 - 3.68 \times 10^{-6} f + 81.43 & 150k \sim 2538k \\ -1.24 \times 10^{-14} f^2 + 6.47 \times 10^{-7} f + 78 & 2538k \sim 30Meg \end{cases} \qquad (10)$$

Comparison of the measured and calculated impedance curves is shown in Figure 3.

In practice, multiple cells are used in series to raise the

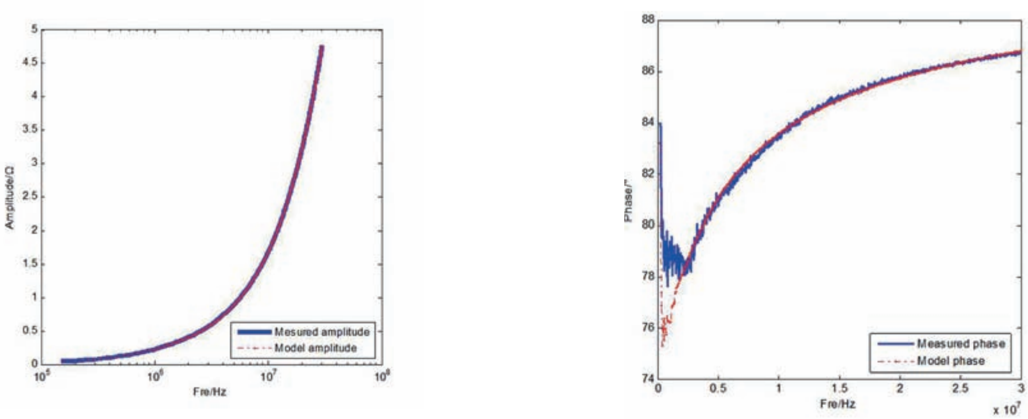

Figure 6: Comparison of measured and simulated impedance curves for a single cell battery: (a) amplitude-frequency; (b) phase-frequency

output voltage. Therefore, we also analyzed cells connected in series; the amplitude-frequency characteristics are as follows:

$$Z(f) = 4 \times Z_0(f) - k_s(f) \quad (11)$$

where $k_s(f)$ is the correction factor caused by wire inductance, and has to be considered:

$$k_s(f) = 2.4 \times 10^{-7} f + 0.01 \quad (12)$$

Comparison of the measured and calculated impedance curves is shown in Figure 4.

Circuit Model Based On Battery Structure

At low frequencies, current density distribution inside a conductor is uniform, whereas at high frequencies current density on the conductor surface becomes large, with almost no current flowing in the conductor's centre; this is called 'skin effect'.

For batteries, when the frequency is above 1kHz, skin effect of the battery's electrodes and connecting wires, along with the impedance of its electrolyte, play a decisive role in its impedance characteristics. Electrode impedance consists mainly of its resistance and inductance. Figure 5 shows the high-frequency impedance characteristic equivalent circuit of the battery, where R_0 is the equivalent resistance of the electrolyte, $R_{ac}(f)$ is the equivalent impedance of the electrode, and L is the electrode equivalent inductance. Taking into account the skin effect, the calculations of $R_{ac}(f)$ and L are as follows:

$$R_{ac}(f) = \sqrt{\frac{\mu}{4\pi r^2 \gamma} \bullet f} \bullet l \quad (13)$$

$$L = \frac{\mu_0 h}{4\pi} + \frac{\mu_0}{\pi} \ln \frac{D-R}{R} \quad (14)$$

where μ is the permeability of the electrode, l is electrode length, γ is its conductivity, D is the distance between the two electrodes, and R is the equivalent radius of the electrodes.

Comparison of the simulated and measured impedance curves is shown in Figure 6.

Model parameters of the battery cells in series are $R_{series} = 4\times(R_0 + R_{ac}(f)) - k_1$ and $L_{series} = 4\times L - k_2$, where $k_1 = 0.046$ is the correction factor for the resistance value of the batteries in series, and $k_2 = 1.865\times10^{-8}$, the correction factor for their inductance value. Figure 7 compares the simulated and measured impedance values.

Circuit Model Based On Vector Fitting

It is well-known that batteries can only function as a DC source. If an AC signal is applied to a battery, it can be treated as a two-port passive component, and we can use a transfer function to represent its port properties. The rational approximation of a transfer function F(s) can be written as Equation 15:

$$F(s) = d + se + \sum_{k=1}^{N} \frac{res_k}{s - p_k} \quad (15)$$

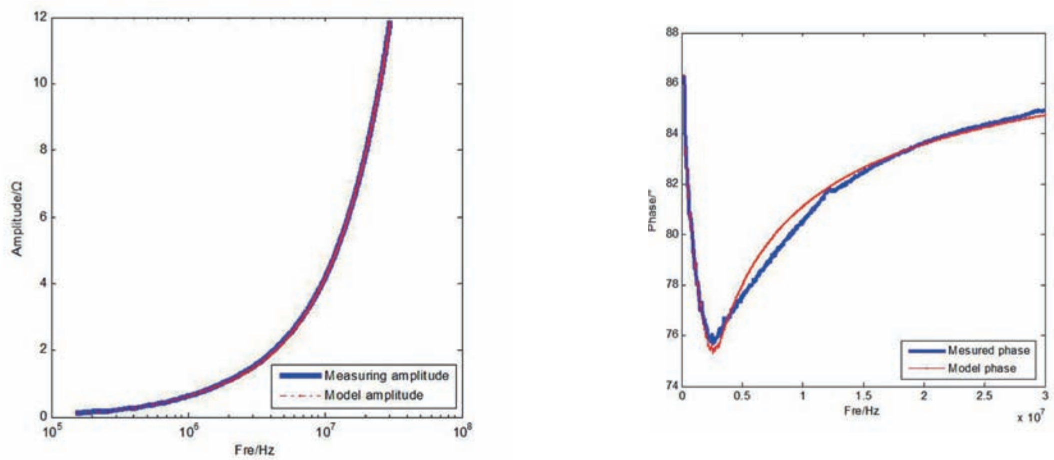

Figure 7: Comparison of the measured and calculated impedance curves for cells connected in series: (a) amplitude-frequency; (b) phase-frequency

where $s = j\omega t$, the complex frequency, res_k and p_k the k th residue (as per the residue theorem, used for evaluating line integrals of analytic functions over closed curves) and pole, which have been extracted by using the fitting process:

(1) The transfer function has real poles. Let us consider the series RL circuit to synthesize the function; the RL admittance of a series RL circuit is Equation 16:

$$Y_{RL}(s) = \frac{I(s)}{V(s)} = \frac{1}{R + sL} = \frac{1/L}{s + R/L} \qquad (16)$$

Its pole and residue are $p_{RL} = -R/L \; res_{RL} = 1/L$; then R and L can be computed.

(2) The transfer function has complex pole pairs. Let res_1, res_2, p_1 and p_2 be pairs of complex and conjugate residues and poles, respectively. The corresponding transfer function F(s) is as per Equation 17:

$$\begin{aligned} F(s) &= \frac{res_1}{s - p_1} + \frac{res_2}{s - p_2} \\ &= \frac{(res_1 + res_2)s - (res_1 p_2 + res_2 p_1)}{s^2 - (p_1 + p_2)s + p_1 p_2} \end{aligned} \qquad (17)$$

An alternative lumped circuit synthesizing a complex pole pair is obtained by comparing the input admittance Y(s) of the circuit shown in Figure 8.

$$Y(s) = \frac{1}{L}\frac{(s + 1/R_2C)}{\left(s^2 + (R_1/L + 1/R_2C)s + (R_1/LR_2C + 1/LC)\right)} \qquad (18)$$

The following relations can then be established:

$$res_1 + res_2 = 1/L \qquad (19)$$

$$-(p_1 + p_2) = R_1/L + 1/R_2C \qquad (20)$$

$$p_1 p_2 = R_1/LR_2C + 1/LC \qquad (21)$$

$$res_1 p_2 + res_2 p_1 = 1/LR_2C \qquad (22)$$

So, R_1, R_2, C and L can then be calculated.

The circuit model of the battery is shown in Figure 9.

The parameters of each element are shown in Table 1.

Figure 10 compares the simulated and measured impedance curves.

Circuit models allow us to simulate the vehicle's electromagnetically-compatible circuits, whereas circuit models based on vector fitting offer greater accuracy. Creating a high-frequency model permits prediction of the conducting behaviour of the battery, including high-frequency losses and the role batteries play in spreading EMI, as well as the external electric and magnetic fields they generate. In addition to modeling the batteries' EMI behaviour as part of a system-level simulation, results give an insight into their electromagnetic effects. ●

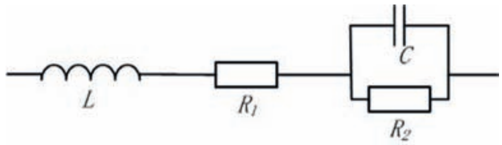

Figure 8: Series equivalent circuit for a complex pole pair

R1	3.99	L1	1.47u
R2	-11.70	L2	1.43u
R3	-6.44	L3	5.40m
R4	19.40k	C1	25n
R5	1.45k	C2	-0.2n

Table 1: Circuit model parameters

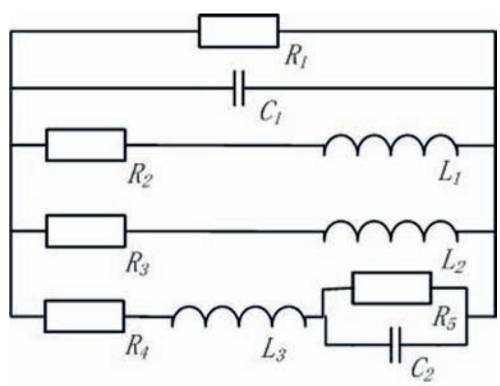

Figure 9: Circuit model for a single cell

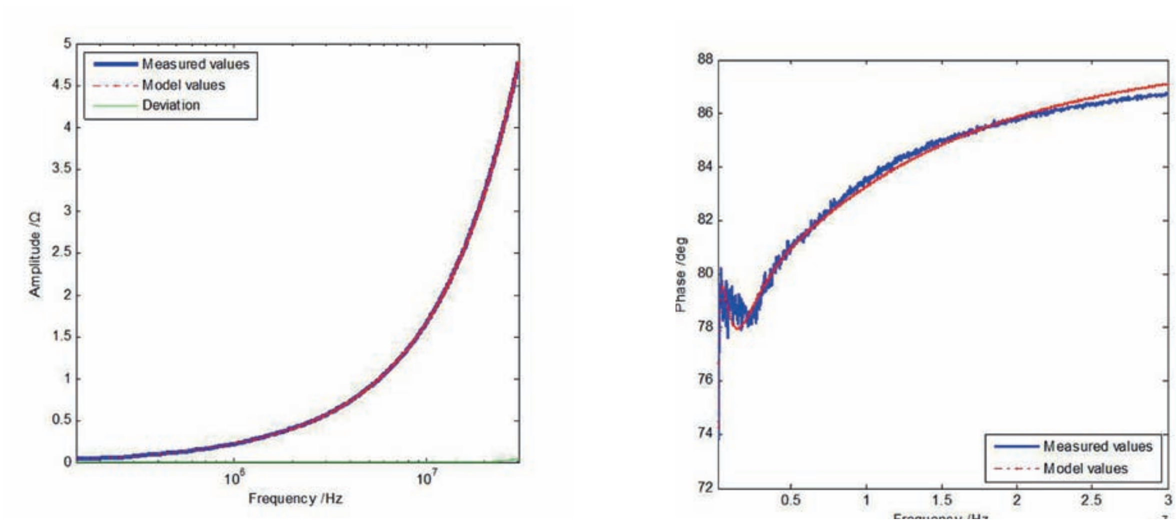

Figure 10: Comparison of measured and simulated impedance curves for a single cell:
(a) amplitude-frequency; (b) phase-frequency

REACTIVE POWER MEASUREMENT USING A VIRTUAL SYNCHRONOUS DETECTOR

AYARI AHLEM, AMIRA HADDOUK AND **HAFIDH MECHERGUI** FROM THE UNIVERSITY OF TUNISIA DESCRIBE A METHOD FOR ACCURATELY MEASURING THE ACTIVE AND REACTIVE POWER OF A SINGLE-PHASE NON-LINEAR LOAD

The ever-growing energy consumption and the increased use of non-linear electrical loads have led us to having to precisely control power sources to optimize their energy efficiency, especially nowadays with the growing use of renewable energy sources.

Electrical power can be considered to have two parts: active power, responsible for the load's operation, and reactive power which develops the magnetic field in the windings. Reactive power needs to be measured when evaluating energy waveform quality (current and voltage) and, in recent years, various methods have been developed for measuring this part of sinusoidal sources typically obtained from solar or wind energy.

For the calculation of electrical power, given by the formula $P = UI\cos\varphi$, researchers are generally inclined to determine the phase angle φ between the voltage and current load, using a zero crossing detector (ZCD). However, this method tends to incur errors.

In this article, we present a new electrical reactive-power measuring method based on a virtual synchronous detector (VSD), where a ZCD is not required because the phase angle between the voltage and current load is not needed for the calculations.

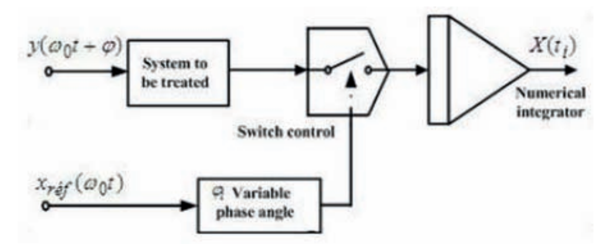

Figure 1: Block diagram of the instrumental synchronous detector

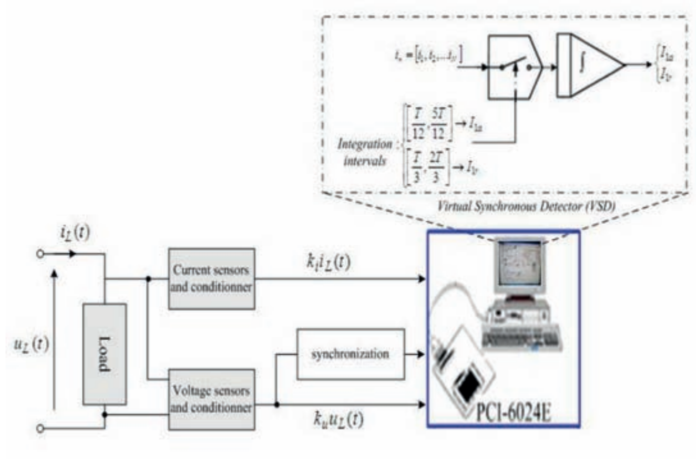

Figure 2: Block diagram of the proposed electric-power measuring instrument

Synchronous Detection Method

In general, a synchronous detection method is used to extract a useful signal buried in noise. The conversion function of the synchronous detector is:

$$Y(t_i) = \frac{1}{T}\int_{t_i}^{t_i+\frac{T}{2}} x(t)dt = \frac{2}{T}X(t_i) = 2.f.X(t_i) \qquad (1)$$

with $x(t) = x(t+T)$ and $x(t) = -x(t+\frac{T}{2})$

where t_i is the initial time synchronous to the reference voltage of the source supplying the load.

The block diagram of the synchronous detector is shown in Figure 1 and it includes:

- A source providing a sinusoidal reference signal;
- A variable phase shifter for selecting the time control t_i or phase angle φ_i;
- A control logic multiplier;
- A digital integrator.

By varying the phase φ_i in the block diagram of Figure 1 we can identify the useful parameters of the electrical load supplied by the network source. Moreover, using Equation 1 we can extract the active and the reactive components Y_a and Y_r of the useful signal:

$$Y_a = \frac{1}{T}\int_0^{\frac{T}{2}} x(t)dt = \frac{X_m}{\pi}\cos\varphi \tag{2}$$

$$Y_r = \frac{1}{T}\int_{\frac{T}{4}}^{\frac{3T}{4}} x(t)dt = \frac{X_m}{\pi}\sin\varphi \tag{3}$$

The synchronous detector is used to determine the active and reactive current of a non-linear load. For linear loads, these measurements are much easier.

So, for a non-linear load, the voltage network is:

$$u_L(t) = U_m \sin(\omega t) \tag{4}$$

and the non-linear load current is:

$$i_L(t) = I_{1m}\sin(\omega t + \varphi_1) + \sum_{k=1}^{\infty} I_{(2k+1)m}\sin((2k+1)\omega t + \varphi_{2k+1}) \tag{5}$$

$$k = 1,2,....,\infty$$

Therefore, the total power consumed by the load is:

$$p_L(t) = u_L(t) \times i_L(t)$$

$$p_L(t) = U_m \sin(\omega t) \times \left[I_{1m}\sin(\omega t + \varphi_1) + \sum_{k=1}^{\infty} I_{(2k+1)m}\sin((2k+1)\omega t + \varphi_{2k+1})\right]$$

$$\begin{aligned} p_L(t) = U_m I_{1m}\sin^2(\omega t)\cos\varphi_1 + U_m I_{1m}\sin(\omega t)\cos(\omega t)\sin\varphi_1 + \\ U_m \sin(\omega t) \times \sum_{k=1}^{\infty} I_{(2k+1)m}\sin((2k+1)\omega t + \varphi_{2k+1}) \end{aligned} \tag{6}$$

If the interval integration is $t_i \in \left[\frac{T}{12}, \frac{5T}{12}\right]$, we can determine the active component of the first harmonic I_{1a}:

$$I_{1a} = \frac{1}{T}\int_{t_i}^{t_i+T/3} i_L(t)dt = \frac{I_{1m}\sqrt{3}}{2\pi}\cos\varphi_1 = \frac{I_{1am}\sqrt{3}}{2\pi} \tag{7}$$

If the integration interval is $t_i \in \left[\frac{T}{3}, \frac{2T}{3}\right]$, we can determine the reactive component I_{1r}:

$$I_{1r} = \frac{1}{T}\int_{t_i}^{t_i+T/3} i_L(t)dt = \frac{I_{1m}\sqrt{3}}{2\pi}\sin\varphi_1 = \frac{I_{1rm}\sqrt{3}}{2\pi} \tag{8}$$

Using Equations 7 and 8, we can determine the amplitude of the first harmonic:

$$I_{1m} = \sqrt{I_{1am}^2 + I_{1rm}^2} \tag{9}$$

Moreover, the active and reactive power elements for the first harmonic are given as:

$$P_1 = U_{rms} \cdot \frac{I_{1am}}{\sqrt{2}} \tag{10}$$

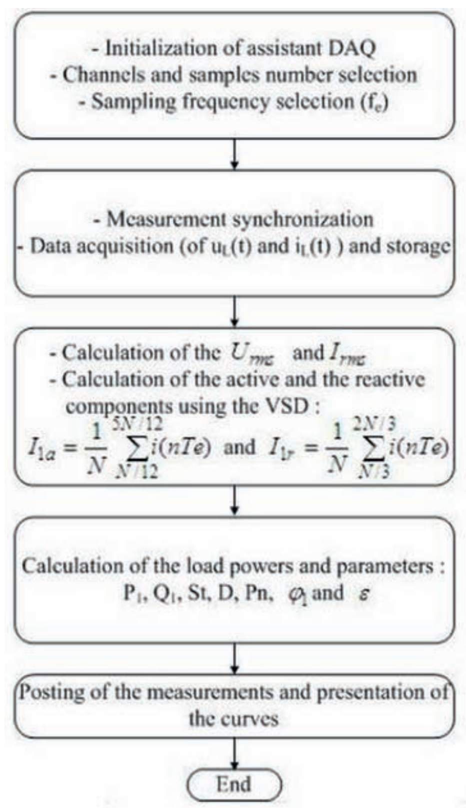

Figure 3: Flow chart illustrating the system's operation steps

and

$$Q_1 = U_{rms} \cdot \frac{I_{1rm}}{\sqrt{2}} \tag{11}$$

This study means we can build a synchronous filter with a sensitivity of $\frac{\sqrt{3}}{2\pi}$, and to determine the active, reactive and apparent power ($S_t = U_{rms} I_{rms}$), as well as deduce the deformation factor $D = \frac{P_1}{S_t}$.

Once the acquisitions samples of $u_L(t)$ and $i_L(t)$ are taken, we calculate U_{rms} and I_{rms}, multiplying them together to yield the real power over the stated interval of time.

The power P_n is calculated as:

$$P_n = \frac{\sum_{j=1}^{N} u_L(jTe) \times i_L(jTe)}{N} \tag{12}$$

where N is the number of samples.

Experimental Validation with LabView

Nowadays many measurement devices use microprocessors to enhance their capabilities and increase their flexibility. The basic

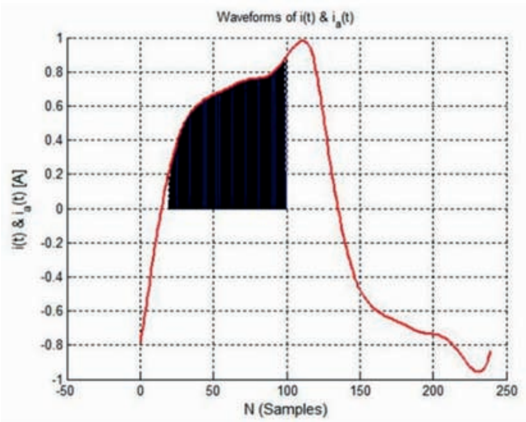

Figure 4: The load current waveform and the active current I_{1a}

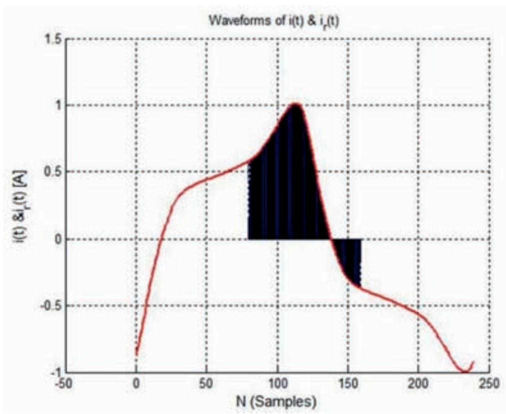

Figure 5: Zero control logic

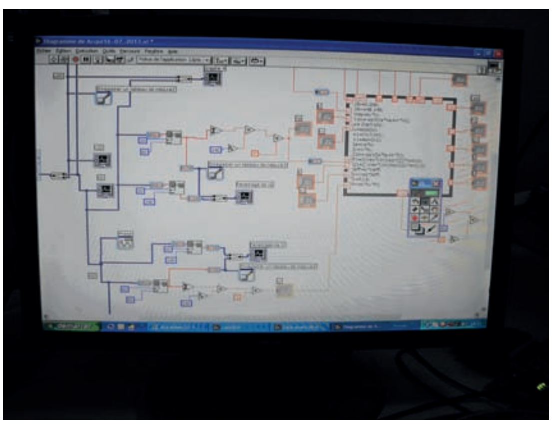

Figure 6: The acquisition diagram using LabVIEW

setup of a circuit used to measure the electric power is an analog circuit responsible for the signal conditioning, followed by an analog-to-digital converter (ADC) and a microprocessor or microcontroller to manipulate the information.

In our setup we used the LabVIEW software to build an instrumental platform that works as a virtual synchronous detector (see the setup in Figure 2). There are two Hall-effect sensors used for the voltage and current part of the system; their signals are then fed to a PC via a PCI-6024E board as illustrated in Figure 2.

We acquire the two quantities $k_v u_L(t)$ and $k_i i_L(t)$. A digital processing algorithm, performing a VSD with LabVIEW, manages the measurement sequences; the calculation of U_{rms}, I_{rms}, I_{1a}, I_{1r}; the determination of different measurement parameters of the load and displays P_1, Q_1, S_t, φ_1, D; as well as the representation graphs (the operation sequences are illustrated in Figure 3).

Figure 4 shows the active current and load current waveforms obtained using the synchronous detection for an integration time of $\left[\frac{T}{12}, \frac{5T}{12}\right]$.

Figure 5 shows the current obtained using the synchronous detection method for an integration time of $\left[\frac{T}{3}, \frac{2T}{3}\right]$.

U_{rms} and I_{rms} are the load voltage and current.

P_1 and Q_1 are the active and reactive power due to the first harmonic.

P_n is the active power, calculated using Equation 12.

S_t is the total apparent power ($S_t = U_{rms}.I_{rms}$).

$$I_{rms} = \sqrt{\sum_{i=1}^{\infty} \frac{I_{1m}^2 + I_{2m}^2 + \ldots}{2}}$$

$\varphi_1 = a\tan(\frac{I_{1r}}{I_{1a}})$, or the phase angle due to the first harmonic.

$I_{1m} = \sqrt{I_{1a}^2 + I_{1r}^2}$, or maximum value of the first harmonic.

D is the load deformation factor.

Equations 10 and 12 are compared to validate the VSD proposed method. Relative error due to this method is $\varepsilon(\%) = \frac{P_n - P_1}{P_{n-scale}} \times 100$, which is around 0.003% (or 30ppm), due to the digital method used by the virtual synchronous detector. This remarkable result confirms that synchronous detection can be a useful part of the synchronous filter. ●

A NEW PER-PHASE CONTROL SCHEME FOR THREE-PHASE FOUR-LEG GRID-CONNECTED INVERTERS

BY **MOHAMMAD REZA MIVEH, MOHAMMAD FADLI RAHMAT** AND **MOHAMMAD WAZIR MUSTAFA**
OF THE FACULTY OF ELECTRICAL ENGINEERING AT UNIVERSITI TEKNOLOGI MALAYSIA

Voltage source inverters (VSIs) are key components of microgrids, because they provide advantages such as power quality, reliability and flexible control for power systems. In recent years, there has been increased interest in three-phase four-leg VSIs due to the benefits they offer to the three-phase four-wire distribution systems and microgrids.

Microgrids

A microgrid can be defined as a cluster of distributed energy resources (DERs) and loads that interface with distribution networks. DERs are usually connected to the distribution network through power electronic devices to provide control. Recent developments in green power have heightened the use of micro-sources such as wind turbines, fuel cells, hydro and PVs integrated with storage devices.

The microgrid can operate in both grid-connected and islanded mode. In grid-connected mode (see Figure 1), the microgrid either imports power from the grid or exports to it, depending on power generation and power consumption, as well as the market and local government policies. The microgrid can also be disconnected from the grid, whenever there's power quality compromise in the energy supply.

DERs often consist of the source, which is connected to inverters to generate direct current (DC) and convert it to alternating current (AC). The most important role of inverters in grid-connected mode is to control the power flow between the utility and the microgrid. In this mode, the output active and reactive power in the VSIs should be adjusted based on pre-specified values; therefore, the VSI should be in power control mode. The main purpose of control is to achieve zero steady-state error, ensuring high power quality and improving transient response.

Controlling the Microgrid

Several techniques have been offered in the literature for controlling the microgrid, which can be categorized as linear and nonlinear. Linear control techniques include proportional

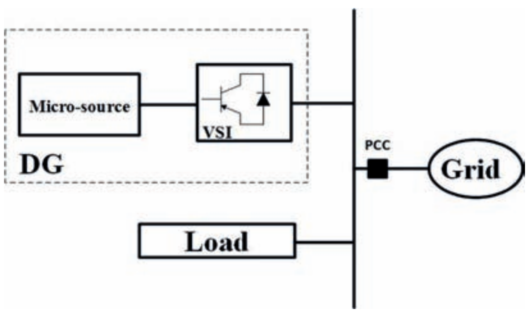

Figure 1: Typical grid-connected microgrid structure

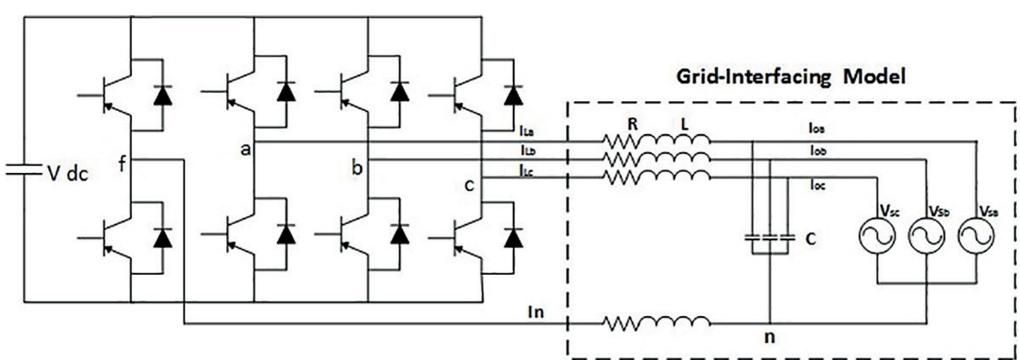

Figure 2: Three-phase four-leg grid-connected VSI model

integral (PI) controllers, proportional resonant (PR) controllers, state feedback controllers and predictive control strategies. Non-linear techniques include hysteresis current controllers (HCCs) and online-optimized controllers.

PR controllers are commonly used because they are capable of eliminating steady-state error; however they cannot cope with varying utility frequency.

The HCC is also a popular control method and, here, the AC current keeps within the limits of a hysteresis band. However, its switching frequency is variable and relies on load and system parameters. Moreover, it cannot cope with unbalanced and nonlinear currents.

Although in recent years there has been an increased interest in nonlinear controllers, they are quite complicated. On the other hand, linear techniques such as PI controllers are widely used and can provide high quality sinusoidal waveforms. These controllers offer extremely good dynamics, overload rejection and low current ripple.

In this article we present a new, per-phase control scheme for a three-phase four-leg VSI operating in grid-connected mode. The suggested control scheme in each phase contains a power controller and a current control loop based on the conventional PI-type regulators in the dq frame (in electrical engineering, direct-quadrature transformation is a mathematical transformation that rotates the reference frame of three-phase systems to simplify the analysis of three-phase circuits). Furthermore, in order to achieve higher dynamic response, feed-forward (FF) compensation is used for the inner current loop.

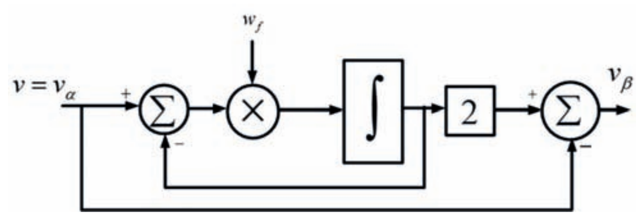

Figure 3: Structure of a first order APF

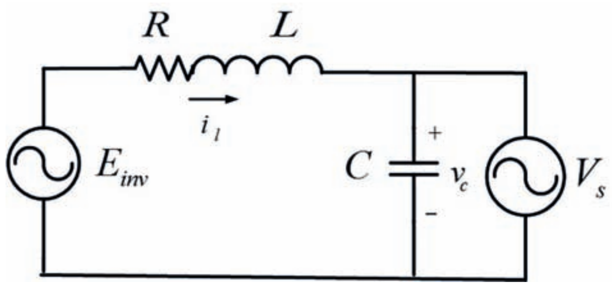

Figure 4: The basic model of a per-phase four-leg inverter

System Modeling

A typical model of a three-phase four-leg grid-connected VSI and its output LC filter is shown in Figure 2, where L and

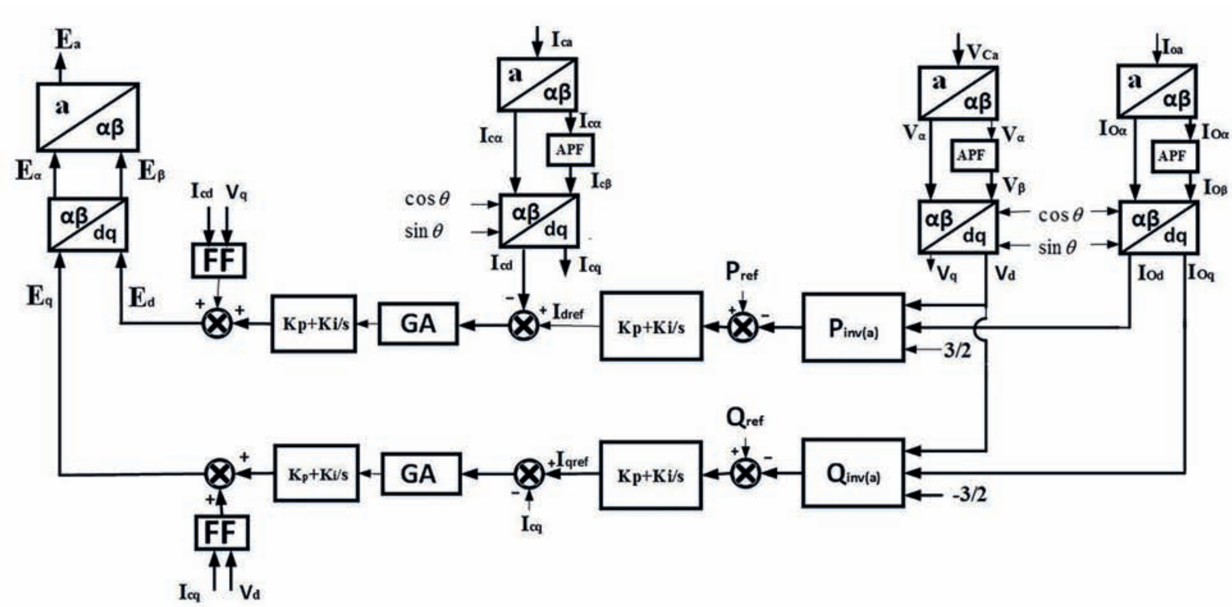

Figure 5: The suggested power control scheme

Option	Value
Population Initial Range	[0,1]
Population Size	30
Generation	1000
Stall Generation	150

Table 1: Parameters of the Genetic Algorothm

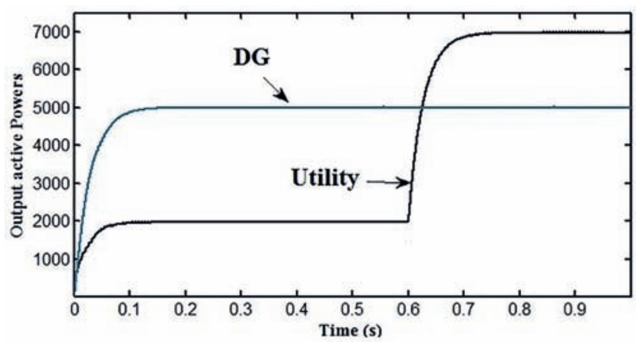

Figure 6: Output active power of the microgrid at load change

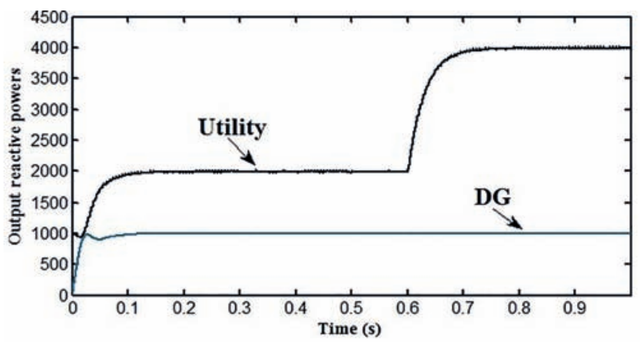

Figure 7: Output reactive power of the microgrid at load change

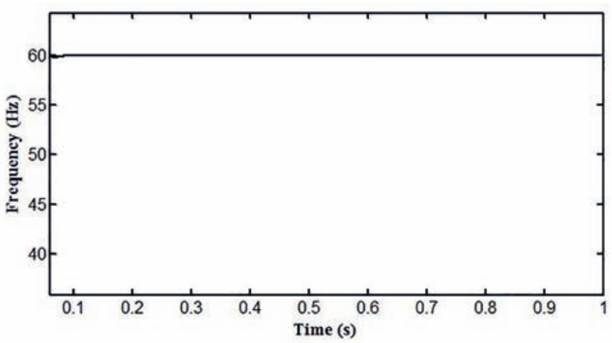

Figure 8: Frequency of the microgrid

R denote the inductance and resistance of the filter, V_s is the utility voltage and C is the filter capacitance. It's worth noting that the neutral point of the microgrid is connected to the fourth leg of the inverter through a fourth inductor. Moreover, by using a sufficiently large capacitance at the DC link, the voltage can be assumed to be constant. In this work, sinusoidal pulse-width modulation (SPWM) is used.

Although controlling single-phase and three-phase inverters in the dq frame is now a widely used method, for three-phase four-leg inverters it is not as well developed as for single- and three-phase applications. This is because each phase must be controlled independently, so the per-phase control scheme for four-leg inverters needs a secondary orthogonal signal in the dq frame. Several orthogonal signal generation techniques have been proposed to generate an orthogonal signal from an original signal. In this study, an all-pass filter (APF) is selected because of its simplicity. Figure 3 shows the structure of a first order APF, where w_f is the fundamental angular frequency.

In order to implement a per-phase control scheme based on orthogonal current components, the fundamental of the switched voltage of one phase of the inverter is modeled as an ideal controlled voltage source (E_{inv}). Figure 4 shows the model of per-phase four-leg inverter based on single-phase calculation. The grid-interfacing model connected to that phase of inverter can be represented by a voltage source (V_s), with the inverter inductor current and capacitor voltages being i_l and v_c respectively.

By using the Clarke transformation (a mathematical transformation used to simplify the analysis of three-phase circuits, also known as the αβ transformation), the equations of the system in Figure 4 in the stationary frame of reference (used to analyze induction motor parameters such as torque and speed) can be derived as:

$$l\frac{di_{l\alpha\beta}}{dt} = e_{inv\alpha\beta} - i_{l\alpha\beta}R - v_{c\alpha\beta} \quad (1)$$

By applying Park's transformation, Equation 1 can be expressed in the dq frame as:

$$\begin{pmatrix} \frac{di_d}{dt} \\ \frac{di_q}{dt} \end{pmatrix} = -\frac{R}{L}\begin{pmatrix} i_d \\ i_q \end{pmatrix} + \frac{1}{L}\begin{pmatrix} e_d \\ e_q \end{pmatrix} - \frac{1}{L}\begin{pmatrix} v_d \\ v_q \end{pmatrix} + w\begin{pmatrix} i_q \\ -i_q \end{pmatrix} \quad (2)$$

where w is the coordinate angular frequency.

The Suggested Control Scheme

As shown in Figure 5, the proposed control scheme in each phase comprises a power control loop, an inner current control loop and a GA block. V_{ca} and I_{ca} are the "a" phase voltage and current of the filter capacitor, respectively. As shown in Figure 5, the α components are created by an a-to-αβ transformation block as a real per-phase component. On the contrary, the β components are created from a theoretical circuit. A simple Phase Locked Loop (PLL) can be applied to detect the voltage phase angle.

As seen in Figure 5, the capacitor current is applied as feedback signal to the current controller, as it provides better disturbance rejection than the inductor current. This is because the capacitor current is directly proportional to the time change of the output voltage, so consequently it gives better prediction of voltage distortion. An FF loop is also applied to avoid coupling between the active and reactive power. Furthermore, conventional PI-type controllers are used for the power and current controllers.

The balance between energy generation and consumption is an important component in the control of microgrids. Moreover, an accurate power exchange between utility and microgrid in the grid-connected mode must be achieved by a proper control scheme to ensure voltage and frequency stability.

> "The balance between energy generation and consumption is an important component in the control of microgrids

Recently, the PQ (active and nonactive/reactive power control) mode has attracted more attention because of the benefits it offers, including either importing less power from the utility in the grid-connected mode or generating stable active and reactive power in the VSIs. It should be noted that the PQ mode is used for DG (distributed generation) units that supply constant power, thus such DG units inject pre-specified active and reactive power.

In this work, the PQ control technique is applied to generate the reference current vectors. The main purpose of using power control scheme is to share active and reactive power requirements of loads among the DG units and the utility supply. In Figure 5, the right side shows the block diagram of the suggested power controller based on a conventional PI-type controller. As seen in the figure, the outer control loop is applied to generate the reference signals i_{dref} and i_{qref}. Note that P_{ref} and Q_{ref} are either set to pre-specified values or are requested by remote control.

In this study, the PQ control technique based on voltage-orientated control is suggested for a three-phase, four-leg inverter. Control of active and reactive power is the main purpose of this controller and must continue in grid-connected modes and during load changing conditions.
In PQ mode, decoupling between the active and reactive power has been accomplished by an FF loop. Moreover, the outputs of the VSI's active and reactive power are regulated based on their reference preset or requested values, and the conventional PI-type controllers make the control parameters available to the reference current vectors. In other words, power errors are tracked by the PI controller to create control variables for the current controllers. Based on the PI controller in the dq frame, the active and reactive power can be obtained as:

$$p = \frac{3}{2} v_d i_d \tag{3}$$

$$Q = -\frac{3}{2} v_d i_q \tag{4}$$

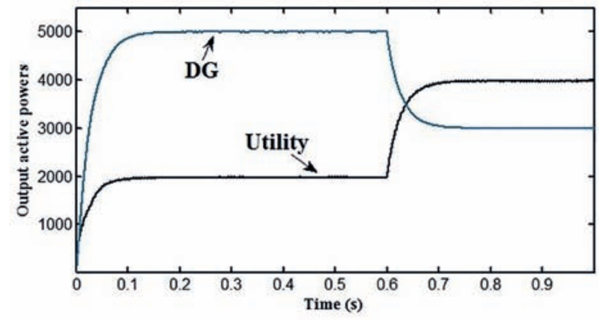

Figure 9: The output active power of utility and DG unit

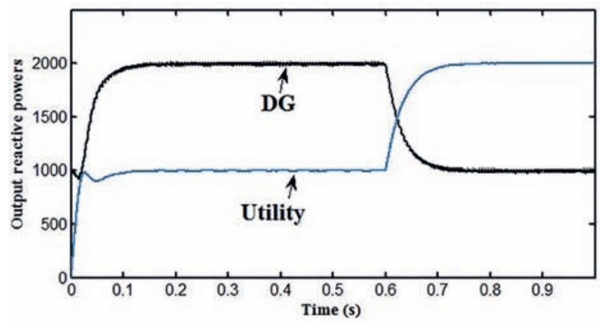

Figure 10: The output reactive power of utility and DG unit

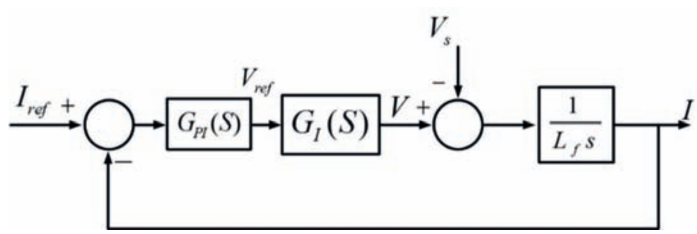

Figure 11: Model of the DG power stage and control system

Also, the reference current vectors can obtained as:

$$i_{dref} = (P_{ref} - P_{inv})(K_{pp} + K_{ip} / s) \quad (5)$$

$$i_{qref} = (Q_{ref} - Q_{inv})(K_{pq} + K_{iq} / s) \quad (6)$$

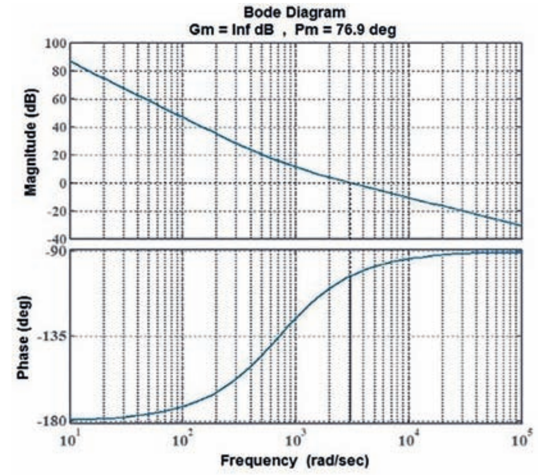

Figure 12: Bode diagram of the current controller

Current Control Scheme

Recently, there has been increased interest in using appropriate inner current-control loops to ensure system stability and improve dynamic performance. Computational intelligence algorithms are attracting attention in addressing power system problems. These methods are categorized based on the objective function and the type of space search. The Genetic Algorithm (GA) is one of the most widely used groups of compensation intelligent algorithms applied to solve power-system problems.

Proposed by J. H. Holland in 1975, the GA can be defined as an evolutionary computation technique that simulates the mechanism of natural selection; a biological method in which stronger individuals are likely to be the winners in a competing environment. Actually, the GA is an iterative algorithm which searches the answers to find the optimal solution for a fitness function. This algorithm assumes that the solution for an objective function is an individual that can be represented by parameters.

> "Recently, there is increased interest in using appropriate inner current-control loops to ensure system stability and improve dynamic performance

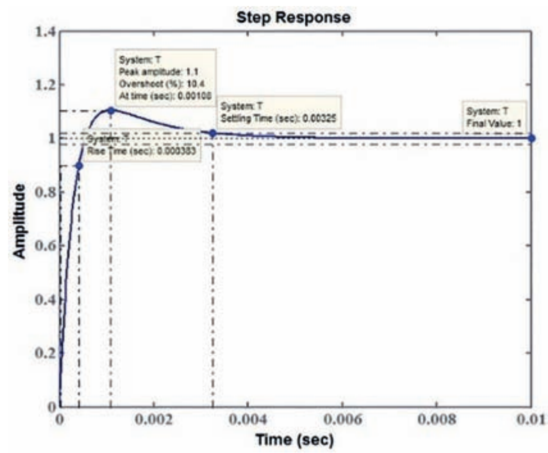

Figure 13: Step-response of the current controller

Nowadays widely used, it can locate a good solution rapidly, so it has been widely implemented because of its simplicity for optimization, with less parameters needed for tuning and robustness.

In this work, GA is incorporated to optimize the current controller's parameters, which means the PI gains of current controllers are optimized to achieve system stability. The fitness function of the GA is based on the integral of absolute error (IAE). The mathematical expression of the IAT performance index is defined by the following equation:

$$IAT = \int_0^\infty t\left|e(t)\right|dt \quad (7)$$

where *t* is time and *e(t)* is the difference between the controlled signal and the reference set-point. Here we consider the minimization of the objective function to find the optimum current control parameters. Table 1 shows the parameters of applied GA.

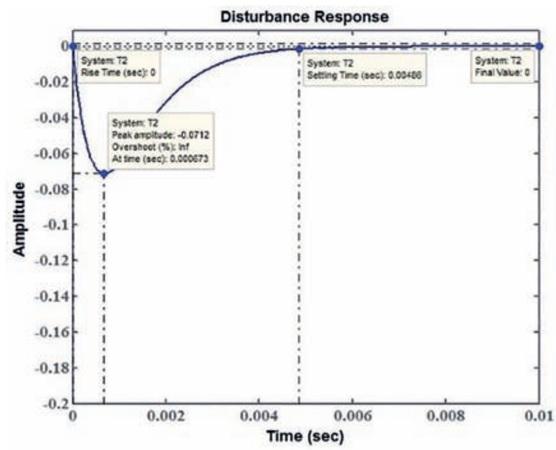

Figure 14: Disturbance response of the current controller

The main task of the current controller is to ensure short transients and accurate signal tracking of the VSI output current. The left side of Figure 5 is the block diagram of the current controllers in the dq frame. Both PI controllers are employed to eliminate current error. In addition, the capacitor feedback loop is used to enhance dynamic and steady-state performance.

Simulation Results

To validate the performance of the suggested control scheme, three-phase four-leg VSI is simulated in MATLAB/Simulink software to investigate its behaviour in the grid-connected mode. The parameters of the DG model we used are l_s= 3.5mH, R_s= 1.15Ω, f = 60Hz, filter capacitance C = 15µF, switching frequency for synchronized pulse width modulation (SPWM) is fixed at 10kHz and sampling frequency is fixed at 500kHz. In this model, the suggested controller is presented based on the PQ method, and the GA algorithm is used to find the optimum current control parameters; the obtained optimal values are

$$K_p^d = K_p^q = 10.411 \text{ and } K_i^d = K_i^q = 7416.$$

In order to validate the performance of the suggested scheme, three simulation case studies were carried out:

1. Load change during grid-connected mode

Here, the grid-connected microgrid of Figure 1 is the test system to evaluate the effectiveness of the suggested controller. A load change has been used to check the response of the utility when the power requirement of the load is less than the power generation of the DG. The set points of the active-reactive power for the PQ-mode-based DG unit are 5kW real and 1kVar reactive power. Also, the load is set to 7kW active and 3kVar reactive power as initial operating points. At 0.6s the load is increased to 12kW active and 5kVar reactive power. It is requested that after 0.6s the balanced power would be supplied by the utility.

Figures 6 and 7 show the variation of active and reactive power of the utility during the load change condition, whereas the DG unit injects a constant output active and reactive power. The frequency of the grid-connected microgrid during load change is shown in Figure 8. As seen, the power flow and frequency are controlled perfectly, and the load is shared between utility and DG unit effectively. Initially, the utility injects 2kW active and 2kVar reactive power into the microgrid; after 0.6s its active and reactive power are increased to 7kW and 2kVar. As it can be seen, the proposed control scheme has the ability to control the power flow during load change.

2. Set-point change of DG unit during grid-connected mode

In this case, the behaviour of the power control scheme is simulated during changes in active and reactive set points of the DG unit. Load parameters are set to 7kW and 3kVar. Also, 5kW active power and 2kVar reactive power are considered initial operating points for the DG unit. At 0.6s, the set-points of active and reactive power in the PQ mode are changed to 3kW and 2kVar respectively. As shown in Figure 9, the active power of the DG unit is decreased to 3kV, thus the balanced power is supplied by the utility, which means the active power of the utility has increased to 4kW.

Figure 10 shows the output reactive powers of the utility and the DG unit. It can be seen that the reactive power of the DG unit has decreased to 1kVar, while the reactive power of the utility has increased to 2kVar. So, the proposed controller offers satisfactory and stable power-flow between microgrid and utility. The proposed control scheme is excellent in controlling power flow during changes of set points.

3. Stability analysis

Here, the transfer function of the current controller with optimized PI gains is determined to analyze the stability of the current controller when working in the grid-connected microgrid. Based on Figure 1 and considering that the switching frequency is much higher than the fundamental frequency, the model of the DG power stage and current control system is achieved as shown in Figure 11, where G_{PI} (s) is the transfer function of the current controller. G_I (s) represents the PWM transfer function, usually modeled as a delay element, and the delay of the PWM is neglected, so the closed-loop transfer function of current controller can be obtained as:

$$G(s) = \frac{K_p s + K_I}{L_f s^2 + K_p s + K_I} \quad (8)$$

The Bode diagram of G(s) considering the current control parameters is shown in Figure 12. As seen, the phase margin of the closed-loop transfer function is positive and the system is stable. Also, Figure 13 shows the step response of the current controller.

It can be seen that the values of the rise-time and overshoot are 0.00151 and 13.3%, respectively. The steady-state error is zero, so the system shows good performance.

As shown in Figure 14, a unit step is applied to analyze the response of the current controller to disturbance. The system shows a good response and any disturbance is damped very soon, further confirming the effectiveness of the suggested control scheme.

Thus, the simulation results conclude that the applied scheme:

- Effectively controls the exchange of power flow between microgrid and utility during load change conditions;
- Robustly controls the injected active and reactive power of a three-phase four-leg grid-connected VSI;
- Effectively controls the power flow of the microgrid when the load power is lower or larger than the rated power of the three-phase four-leg grid-connected VSI; and
- Adequately optimizes the current control parameters to ensure system performance. ●

THIS SERIES PRESENTS SOME SIMPLE ARDUINO PROJECTS. ARDUINO IS AN OPEN-SOURCE ELECTRONICS PROTOTYPING PLATFORM, BASED ON FLEXIBLE, EASY-TO-USE HARDWARE AND SOFTWARE

Arduino Control Of DC Motor Speed

BY **JOHN NUSSEY**

Need more control of your DC motor? You can use the MotorControl sketch for the Arduino to gain full control of the motor on the go.

The MotorControl Sketch

To gain control of the speed of the motor, you need to add a potentiometer to the circuit. Therefore you'll need:

- An Arduino Uno;
- Breadboard;
- Transistor;
- DC motor;
- Diode;
- A 10kohm variable resistor;
- A 2.2kohm resistor;
- Jumper wires.

Find a space on your breadboard to place the potentiometer. The centre pin of the potentiometer is connected back to pin 9 using a jumper wire and the remaining two pins are connected to 5V on one side and GND on the other.

The 5V and GND can be on either side, but switching them will invert the value the potentiometer sends to the Arduino. Although the pot uses the same power and ground as the motor, note that they are separate circuits linked through the Arduino.

After you have built the circuit, open a new Arduino sketch and save it with another name, such as myMotorControl, and then type the following code:

```
int potPin = A0;
int motorPin = 9;
int potValue = 0;
int motorValue = 0;
void setup() {
 Serial.begin(9600);
}
void loop() {
 potValue = analogRead(potPin);
 motorValue = map(potValue, 0, 1023, 0, 255);
 analogWrite(motorPin, motorValue);
 Serial.print("potentiometer = " );
 Serial.print(potValue);
 Serial.print("\t motor = ");
 Serial.println(motorValue);
 delay(2);
}
```

After you've typed the sketch, save it and click the Compile button to highlight any syntax errors. If the sketch compiles correctly, click Upload to upload the sketch to your board. When it is done uploading, you should be able to control your motor using the potentiometer. Turning the potentiometer in one direction causes the motor to speed up; turning it the other way causes it to slow down.

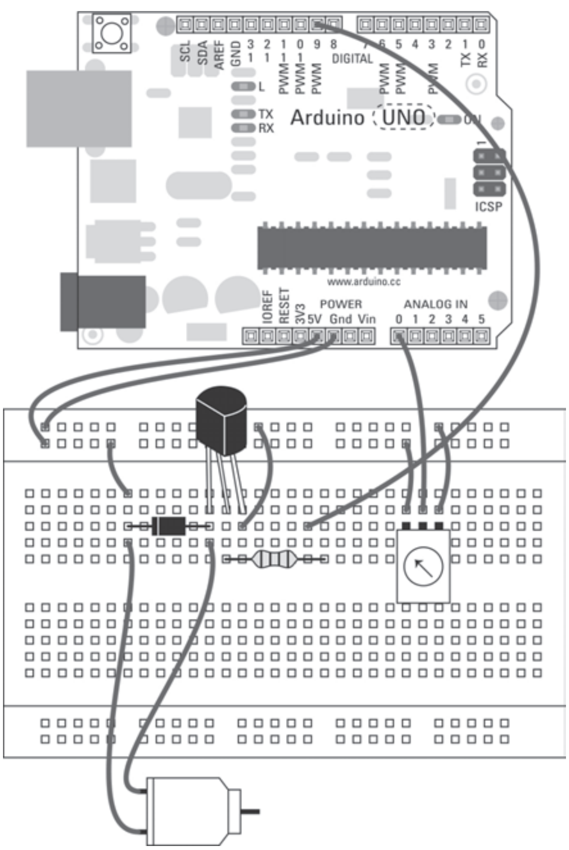

Figure 1: Motor control pictorial diagram

The MotorControl Sketch Breakdown

This sketch is a variation on the AnalogInOutSerial sketch and works in exactly the same way with a few name changes to better indicate what's being controlled and monitored on the circuit.

As always, you declare the different variables used in the sketch. To assign the potentiometer pin use PotPin, and motorPin to send a signal to the motor. The potValue variable is used to store the raw value of the potentiometer and the motorValue variable stores the converted value that you want to output to the transistor to switch the motor.

```
int potPin = A0;
int motorPin = 9;
int potValue = 0;
int motorValue = 0;
```

How To Tweak The MotorControl Sketch

You may find that there is a minimum speed below which the motor will just hum. It does so because it doesn't have enough power to spin. By monitoring the values sent to the motor using the MotorControl sketch, you can find the motor's stall-speed and optimize motorValue to turn the motor within its true range.

To find the range of motorValue, follow these steps:

- With the MotorControl sketch uploaded, click the serial monitor button at the top right of the Arduino window.
  The serial monitor window will show the potentiometer value followed by the output value being sent to the motor, in this fashion:
  potentiometer = 1023 motor = 255
  These values are displayed in a long list and update as the potentiometer is being turned. If you don't see the list scrolling down, make sure the Autoscroll option is selected.
- Starting with the potentiometer reading a value of 0, turn it very slowly until the humming stops and the motor starts spinning.
- Make a note of the value displayed at this point.
- Use an 'if' statement to tell the motor to change speed only if the value is greater than the minimum speed needed to spin the motor, as follows:

WIN THE 'ARDUINO FOR DUMMIES' BOOK BY JOHN NUSSEY

John Nussey is a creative technologist based in London. He teaches interaction design and prototyping at the Goldsmiths College and the Bartlett School of Architecture among others. We have a couple of copies of this book to give away. To enter please supply your name, address and email to the Editor at svetlanaj@sjpbusinessmedia.com. The winner will be drawn at random and announced at the end of the series.

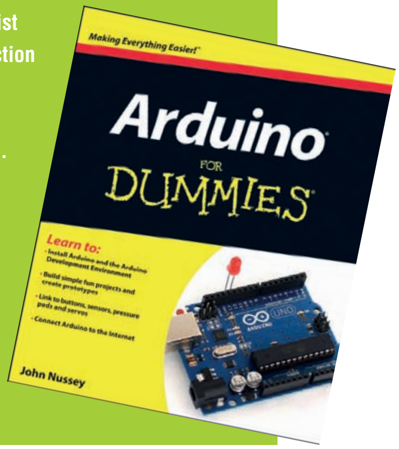

(i) Find the part of your code that writes the motorValue to the motor:

```
analogWrite(motorPin, motorValue);
```

(ii) Replace it with the following code:

```
if(motorValue > yourValue) {
analogWrite(motorPin, motorValue);
} else {
digitalWrite(motorPin, LOW);
}
```

- Now replace yourValue with the number you made a note of. If the value motorValue is greater than that, the motor speeds up; if it is lower than that, the pin is written LOW so that it is fully off. You could also type analogWrite(motorPin, 0) to accomplish the same thing. Tiny optimizations like this can help the project function smoothly, with no wasted movement or values. ●

More on this and other Arduino projects can be found in the book 'Arduino For Dummies' by John Nussey.

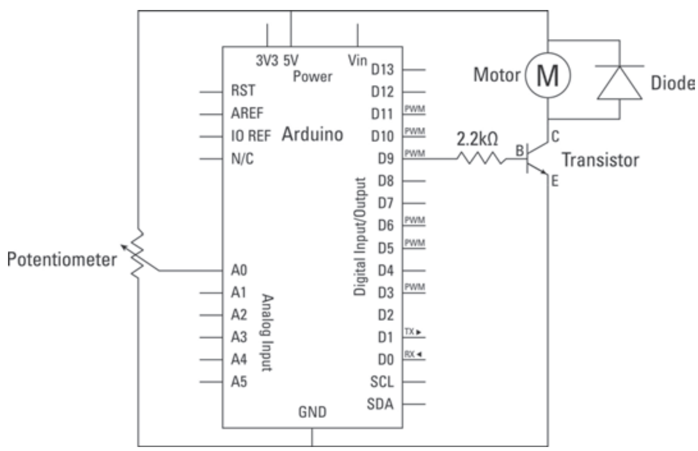

Figure 2: Motor control schematic diagram

Miller Effect

MAURIZIO DI PAOLO EMILIO, PHD IN PHYSICS AND A TELECOMMUNICATIONS ENGINEER, PRESENTS THIS SERIES OF ARTICLES ON THE FUNDAMENTALS OF MICROELECTRONICS

The effective input impedance of an amplifier depends on the impedance connected from input to output. The apparent scaling of this impedance often dominates the input impedance and frequency response of the amplifier; the effect is known as the 'Miller effect'.

First Description

The Miller effect was noticed by John Milton Miller, who was working on vacuum tube triodes when he saw an increase in the equivalent input capacitance of an inverting voltage amplifier. He published his work in 1920, but the same theory applies to modern-day devices, such as bipolar and MOS transistors. This was was later formulated as a theorem. So, Miller's Theorem states that impedance Z connected between two terminals of an N-terminal pair network can be replaced by two impedances Z_1 and Z_2 connected between the same terminals and the reference terminal or ground (Figure 1).

Considering an amplifier with voltage gain A (Figure 2), and impedance Z connected from input to output, the input current can be calculated as:

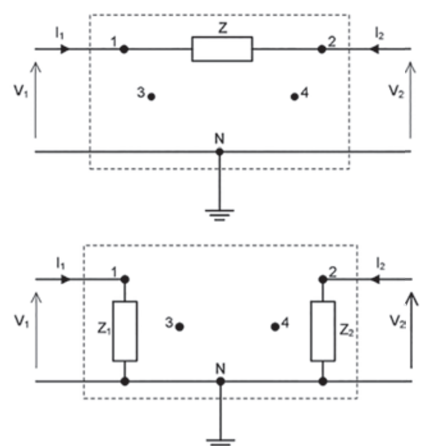

Figure 1: Miller theorem

$$I_i = \frac{V_i - V_0}{Z} = V_i\left(\frac{1+A}{Z}\right)$$

The Thevenin input impedance is:

$$Z_{in} = \frac{V_i}{I_i} = \frac{Z}{1+A}$$

thus a resistor or inductor connected from input to output will be a factor of (1+A) times smaller (as seen from the input terminal), with a capacitance (1 + A) times larger.

In the BJT field, the Miller-effect is nothing else than the feedback of the collector-emitter voltage V_{CE} via the gate-collector capacitance C_{GC} on the gate. This means a change of V_{CE} has the same effect as an internal current source into the bias circuit, where the current is given by:

$$i_g = C_{GC} V_{CE} \frac{dV_{CE}}{dt}$$

Unfortunately C_{GC} is not constant; it changes with V_{CE}.

Effects

As most amplifiers are inverting, the effective capacitance at their inputs is increased due to the Miller effect. This can reduce the bandwidth of the amplifier. The junction and stray capacitances between the base and collector terminals of a Darlington transistor, for example, may be drastically increased by the Miller effect due to corrected gain, lowering the high frequency response of the device.

The Miller effect may be undesired in many cases, and ways may be sought to lower its impact. Several such techniques are used in designing amplifiers, such as a common base may be used as a current buffer at the output of a common emitter stage, forming a cascode. This will typically reduce the Miller effect and increase the bandwidth of the amplifier.

Miller Capacitances

The parasitic capacitance between the input and output electrodes of inverting amplifying devices, such as between the base and collector of transistors, is particularly troublesome

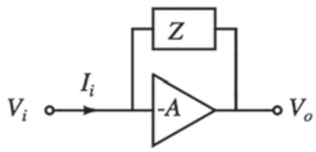

Figure 2: Amplifier (general outline)

because it is multiplied by the gain of the device. This so-called *Miller capacitance* is a major factor limiting the high frequency performance of active devices such as transistors. Assuming the amplifier shown in Figure 2 is an ideal inverting amplifier with voltage gain A, and $Z = C$ is a capacitance between its input and output, then the output voltage of the amplifier is:

$$V_0 = -AV_i$$

and the input current is:

$$i_i = C\frac{d}{dt}(V_i - V_0)$$

So the capacitance at the input of the amplifier is:

$$C_M = C(1+A)$$

The input capacitance is multiplied by the gain of the amplifier; this is the Miller capacitance. If the input circuit has resistance to ground of R_i, then (assuming no other amplifier poles) the output of the amplifier is:

$$V_0 = \frac{A}{1 + j\omega R_i C_M}$$

The bandwidth of the amplifier is limited by the high frequency roll-off at:

$$f = \frac{1}{2\pi R_i C(1+A)}$$

So the bandwidth is reduced by the factor $(1 + A)$.
The effect of C_M on amplifier bandwidth is greatly reduced for low impedance drivers. Consequently, one way to minimize the Miller effect is to use a low-impedance driver, for example by interposing a voltage follower stage between the driver and the amplifier, which reduces the apparent driver impedance seen by the amplifier.

The output voltage of this simple circuit is always $A_v V_0$. However, real amplifiers have output resistance. If the amplifier output resistance is included in the analysis, the output voltage exhibits a more complex frequency response and the impact of the frequency-dependent current source on the output side must be taken into account. Ordinarily these effects show up only at frequencies much higher than the roll-off due to the Miller capacitance, so the analysis presented here is adequate to determine the useful frequency range of an amplifier dominated by the Miller effect.

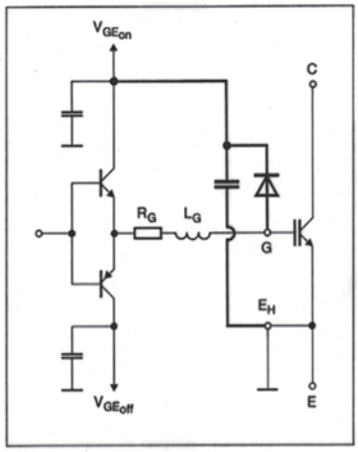

Figure 3: Miller effect in IGBTs: gate clamping

The Miller capacitances will cause the input capacitance on the gate of a FET to appear as a larger capacitance since the charge supplied to the input is now distributed to charging the gate and the drain. The change in the input capacitance is a function of the transconductance of the transistor.

IGBT

Due to the Miller effect, the increase of the collector-emitter voltage causes a current that elevates the gate voltage if the gate cannot be discharged fast enough. This is especially critical when the IGBT is controlled by a source with a series gate resistor. Therefore, it is very important to use a gate clamping in such short-circuit cases (Figure 3). ●

IAN DARNEY PRESENTS A SERIES OF ARTICLES ON CIRCUIT MODELLING FOR ELECTROMAGNETIC COMPATIBILITY

Design Guidelines

This is the final article in this series. Previous articles have identified the key relationships between electromagnetic theory and circuit theory which enable electromagnetic interference (EMI) to be analysed using circuit models. This simplifies the mathematics to a level that can be understood and utilised by any electronics or electrical engineer.

The technique has established a set of mathematical relationships between the geometry of the signal link, its circuit model and the results of bench testing. This approach provides an insight into the underlying physics and enables a set of simple guidelines to be formulated.

Structure As A Shield

The concept of the 'equipotential ground plane' is extremely attractive to engineers involved in the design of systems installed in conductive frameworks such as ships, ground vehicles, aircraft and spacecraft. It is reasoned that, since the structure provides a very convenient return path for signals and power supplies, there is no need to install 'return' conductors that cost money and add mass.

This reasoning ignores the fact that every conductor, including the conducting structure, possesses the properties of inductance and capacitance. Any transient currents in the structure due to power supplies being turned on and off will create high voltages along its length. These voltages will be in series with any low-power signal which also uses the structure as a return path. If every signal uses the structure in this way, then every signal will interfere with every other signal.

In a multi-layer printed circuit board (PCB), the ground plane does seem to behave as an equipotential surface, so it is useful to analyse the behaviour of this conductor in more detail.

Figure 1 illustrates part of a PCB where two adjacent tracks are connected to two voltage sources at the near end and shorted to the ground plane at the far end.

If each of these three conductors is represented as an array of parallel conductors, then the magnetic coupling between each pair of these 'basic' conductors can be used to calculate the current in each one. The distribution of the magnetic field in this simulation will be the same as that of the assembly of Figure 1. The current in each elemental conductor then defines how the current is distributed in the cross-section of each of the three actual conductors. This results in Figure 2.

As expected, the current peaks at the edges of the two tracks, the region where the electromagnetic field is most intense. However, the distribution of current in the ground plane is more interesting. Under the left hand trace, the current is negative; under the right-hand trace, it is positive, so current is flowing in opposite directions in the ground conductor. This will inevitably lead to current loops within the plane and reflections at the boundaries. Electromagnetic waves propagating in different directions in the same region of conducting material are certain to interact. This effect can be compared to the behaviour of sea waves inside a harbour wall, where the water is much calmer.

This calming action is characteristic of all conducting surfaces – the ground plane acts as a shield.

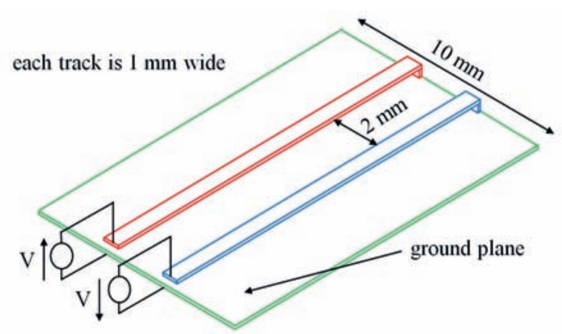

Figure 1: Two printed circuit tracks over a ground plane

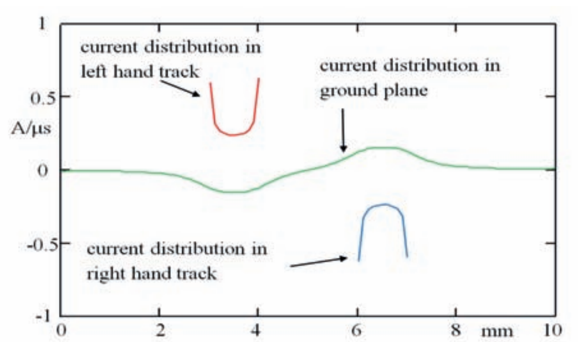

Figure 2: Distribution of a current in cross-section of PCB

So, the first guideline is: *The best use of a conductive structure is as a shield. It should not be used as a convenient return path for any of the signals or power supplies in the system.*

Conductor Pairing

Every conductor acts as an antenna, a statement of the obvious to anyone who owns a car with a whip aerial. That same aerial can also be used to transmit a signal into the environment. Conductors do not magically lose this property when assembled together in a cable harness.

A twin-conductor transmission line can be regarded as a transmitting antenna laid alongside a receiving antenna. The electromagnetic wave carrying the signal is guided along a path bounded by these two conductors. If the two conductors follow entirely separate paths from one item of equipment to another, then the signal link will certainly be extremely susceptible to interference. Equally, power supplies routed in this way will create high levels of radiated interference.

This leads to the second guideline: *Assign a 'return' conductor to every 'send' conductor and keep these two conductors as close together as possible along the entire route from source to load.*

Ground Loops

Figure 3 shows a configuration where three different printed circuit boards are used to process a signal. Each board is supplied with a steady-state voltage of 15V derived from a stabilised supply module. The intent of the configuration is to ensure that all signals are processed with respect to a unique reference, the single-point ground. The reason put forward by advocates of this configuration is that there can be no cross-coupling due to return current flowing in a shared conductor.

When it is recognised that every conductor acts as an antenna, it can be seen that current in every conductor induces an interference voltage into every other conductor, so this configuration guarantees maximum interference. The concept of the single-point ground is well past its sell-by date.

Figure 4 shows how to achieve a dramatic improvement in performance. Since the conductors carrying each signal from board to board are as close together as possible, the electromagnetic wave created by the signal current is constrained to follow the intended path. Any unwanted voltage appearing in one conductor will be matched by an equal voltage injected in the other conductor. This can be simulated by a common-mode voltage, *Vthreat*, appearing in series with the structure. Although this voltage constitutes interference, there are many ways of minimising its effect.

The configuration of Figure 4 introduces a number of 'ground loops'. They have the effect of creating circulating currents which behave in essentially the same way as circulating currents in the ground plane of a printed circuit board; they interact to dissipate unwanted energy. So, the third guideline is: *Create a ground loop wherever that option exists. It will enhance the shielding properties of the system.*

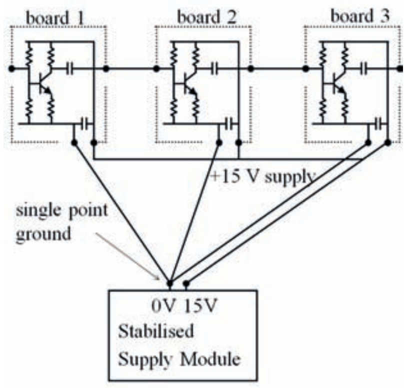

Figure 3: Single-point ground

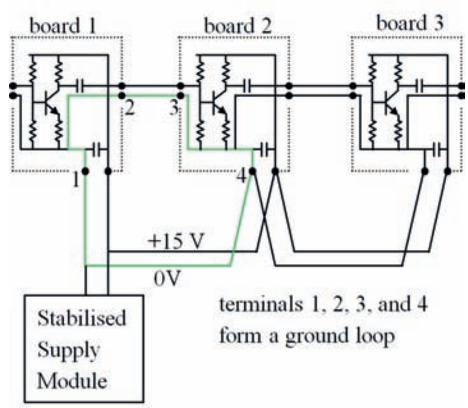

Figure 4: Introduction of ground loops

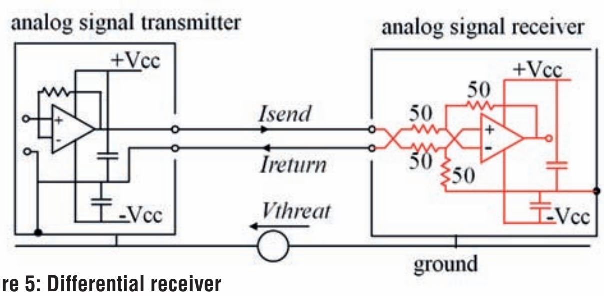

Figure 5: Differential receiver

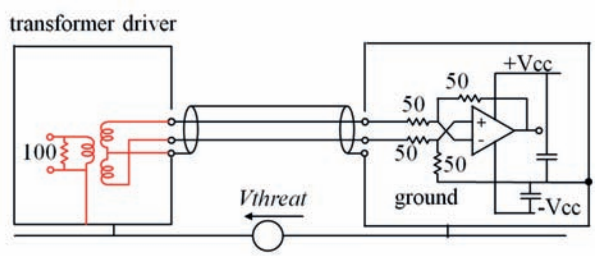

Figure 6: Centre-tapped transformer

Balance

When the system is designed to use two conductors to carry each signal, many ways of enhancing EMC become available. It is sufficient to identify two.

Figure 5 shows how current balance can be achieved in the differential-mode loop. The red operational amplifier generates a current in the return conductor which balances that in the send conductor. The better the balance, the better the common-mode rejection.

Figure 6 shows how a centre-tapped transformer can achieve voltage balance. When a positive voltage is applied to the send conductor, the applied voltage to the return conductor is negative.

So, the fourth guideline is: *Design the interface circuitry to enhance the balance between the currents in the send and return conductors. Ideally, the net current flow in the cable should be zero.*

Differential-Mode Damping

Current carried by a transmission line can be likened to a wave. If this wave is reflected at either termination, energy will be lost from the system and this loss will be in the form of electromagnetic field emissions. Conversely, efficient signal transmission is achieved and the emissions are minimised when there are no reflections. This objective can be met by terminating the line with a resistor equal in value to the surge resistance.

From the point of view of transient behaviour, a capacitor behaves as a short circuit and an inductor behaves as an open circuit; both configurations will create a high level of interference. Figure 7 illustrates ways of dealing with this problem.

So the fifth guideline is: *Design the line terminations to minimise reflections. It is better to dissipate unwanted energy in a resistor than to allow it to radiate into the environment.*

Common-Mode Damping

Reflections are not restricted to the differential-mode loop. They are even more prevalent in the ground loop – the source of common-mode voltages.

Figures 8 and 9 illustrate ways of damping down the resonant peaks in the common-mode current *Icm*.

So the sixth guideline is: *Where necessary, introduce damping into the common-mode loop.*

The Design Process

The preceding six guidelines provide a framework for any electrical system design. If they are implemented at the initial stage of the design process and maintained during the development and manufacturing stages, then the system will have the best chance of meeting the EMC requirements.

Inevitably, there will be conflicts between the need to ensure that the EMC requirements are met and the need to avoid overdesign. It is at this point that the technical approach described in the previous five articles comes to the fore. This approach allows EMC to be dealt with exactly the same way as other design requirements, through analysis, bench testing, review, modification, re-test and final review.

For example, the setup of Figure 8 can be analysed using the circuit model of Figure 10. Component values can be derived from data sheets, geometrical measurements, or individual bench tests. The analysis would be essentially the same as that on a functional module using SPICE software. ●

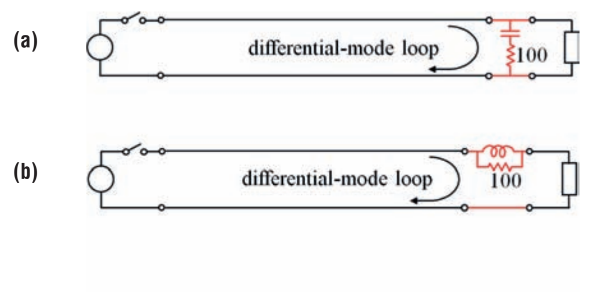

Figure 7: Differential-mode damping, (a) resistor in series with capacitor, (b) restisor in parallel with inductor

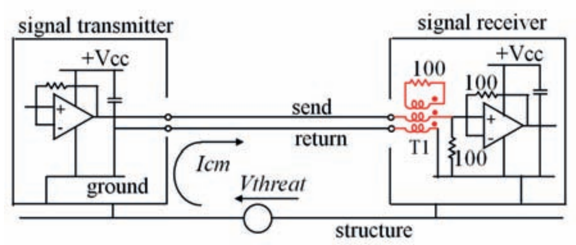

Figure 8: Grounded circuit – damping

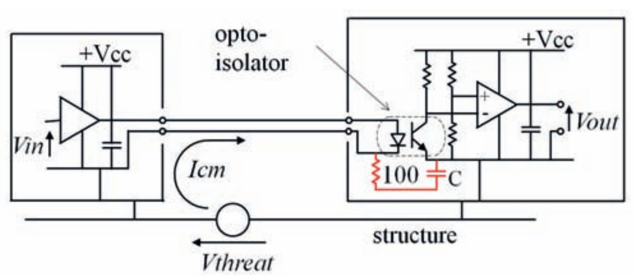

Figure 9: Floating circuit – damping

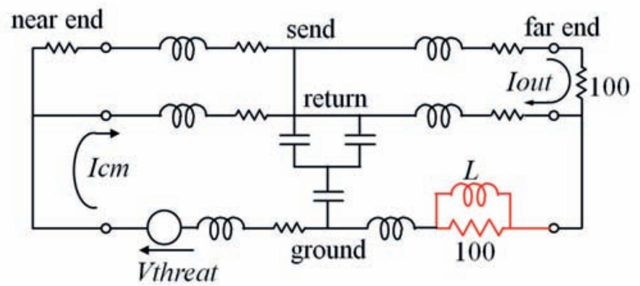

Figure 10: Modelling the setup of Figure 8

TE CONNECTIVITY LAUNCHES M8/M12 CONNECTOR SYSTEM FOR MACHINE INDUSTRIAL AUTOMATION AND CONTROL APPLICATIONS

TE Connectivity (TE) has launched a new connector system for machine industrial automation and control applications. The newly expanded, easy-to-install M8/M12 Connector System offers design engineers a reliable and complete solution to decrease downtime in industrial environments and supports higher bandwidth needs, meeting the requirements of up to 10Gb/s.

The new system includes an extensive range of board and field installable connectors, cable assemblies and IO boxes. Key applications include: industrial automation, automobile manufacturing, machine tooling, semiconductor manufacturing, factory automation machines, vision systems and manufacturing of solenoid and sensor valves. The system is also sufficiently robust for use in harsh commercial applications such as outdoor data communications, outdoor telecoms and advanced traffic monitoring.

Designed to meet IEC-61076-2-101, the new M8/M12 Connector System is also well suited for applications outside the traditional industrial environment, offering benefits wherever a compact reliable connection system with IP67 and IP68 environment protection is required.

Introducing the new product range, Eric Leijtens, global product management leader, TE Connectivity said: "At TE, we understand that different applications and industries have various requirements. However, the one thing they have in common is that the communication needs to work consistently and flawlessly. The new M8/M12 system fully complements our industrial communications portfolio and enables us to offers customers a solution that is time-saving and error-free, both now and in the future."

TE's broad solution provides customers with shielded, unshielded and customized cable assembly options in both Cat5e and Cat6A types, offering different lengths and temperature resistance.

While the passive distribution boxes offer reduced cabling and ease of installation and maintenance, the range of straight, angled, LED, multiposition and high-speed connectors provide a solution for many industrial applications. Additionally, the T and Y adaptors facilitate simple splitting of control signals, allowing versatile systems to be quickly and easily established.

For more information on the new M8/M12 system, please visit www.te.com/products/m8-m12.

www.te.com

ECOC Exhibition

22 – 24 September 2014

Palais des Festivals, Cannes, France

www.ecocexhibition.com

The ECOC Exhibition is the largest European optical communications event and a key meeting place for the fibre optic communication technology community. This year the event comes to Cannes, at the Palais des Festivals from 22 – 24 September, to again provide an unrivalled opportunity for manufacturers, suppliers and service providers of optical communications products and services to meet and network with top decision makers from the industry.

Market Focus 2014

One feature area within the exhibition hall is the Market Focus theatre, sponsored by Oclaro. Now in its ninth successful year, the ECOC Market Focus has grown to become one of the focal points of the show and a popular platform to gain industry knowledge and insight into the latest technologies. The content for the sessions is overseen by a panel of industry experts who are also the decision-making force behind the presentations.

FTTx Centre

Returning to the show in 2014 is the FTTx Centre. This year it will have 11 specialist zones, featuring cutting-edge technologies and interactive engineering demonstrations, including fibre optic network delivery methods and OSP and ISP for FTTx vendor independent products. This runs in conjunction with CTTS Group with zone sponsors that include Anritsu, FTTH Council Europe, ITW Chemtronics and Prysmian Group. CTTS technical experts will be at hand to give detailed explanations of the products on show.

CTTS Training Centre

Once again, the ECOC 2014 exhibition will feature free training sessions led by CTTS. These free hands-on and learning-intensive sessions provide essential insight into key techniques such as modern fusion splicing and passive optical network testing. Places for each session are limited, so register your interest or book your session early to avoid disappointment.

ECOC TV

As before the camera crews of ECOC TV will tour the exhibition and market focus areas inviting views, news and opinions from exhibitors and visitors alike – so do get in front of the camera to talk about your company news or industry views.

The ECOC Exhibition and all feature areas are free to attend and registration is now open. Find out more and plan your visit by going to **www.ecocexhibition.com**

DS1210+	0.99	DS1210+	0.99
DS1302+	0.72	DS1302+	0.72
DS1302Z+	0.79	DS1302Z+	0.79
DS1307+	1.08	DS1307+	1.08
DS1307Z+	0.83	DS1307Z+	0.83
DS18S20+	0.99	DS18S20+	0.99
DS18B20+	1.23	DS18B20+	1.23
DS80C320MCG+	3.35	DS80C320MCG+	3.35
MAX202CPE+	0.81	MAX202CPE+	0.81
MAX202ECPE+	1.19	MAX202ECPE+	1.19
MAX232CPE+	0.69	MAX232CPE+	0.69
MAX485CPA+	0.83	MAX485CPA+	0.83
MAX485CSA+	0.86	MAX485CSA+	0.86
MAX487CSA+	0.75	MAX487CSA+	0.75
MAX487CPA+	0.84	MAX487CPA+	0.84
MAX690CPA+	1.51	MAX690CPA+	1.51
MAX749CSA+	2.31	MAX749CSA+	2.31
MAX7221ENG+	2.32	MAX7221ENG+	2.32
MAX7219EWG+	2.31	MAX7219EWG+	2.31
MAX3232CSE+	0.69	MAX3232CSE+	0.69
MAX13487EESA+	0.53	MAX13487EESA+	0.53

MICROCHIP ANNOUNCES NEW FAMILY OF USB POWER DELIVERY CONTROLLERS

Microchip announces, from Computex Taipei, a new family of USB Power Delivery (UPD) controllers – the UPD100X with industry-standard power delivery and battery charging protocol. A single USB cable can be used for data and simultaneously deliver up to 100W of power from a single standard USB port which is 40 times the power compared to USB 2.0. With up to 100W of available power, designers can dynamically allocate this power to fast battery charging and system power.

The UPD1001 is the first of the family and is a highly flexible and configurable solution that supports the five USB-IF standard UPD power profiles plus an additional 25 UPD-compliant profiles for a total of 30 profiles supported by a single chip. This will allow designers to select the optimum power profiles in order to meet their specific application requirements. Simple configuration is achieved by strapping the two configuration select pins on the UPD1001.

www.microchip.com

TELEDYNE LECROY ANNOUNCES HD4096 TECHNOLOGY BASED OSCILLOSCOPE

Teledyne LeCroy has announced the HDO8000 oscilloscope product line with 8 analog input channels and 12 bits of vertical resolution based on its HD4096 technology. The HDO8000 oscilloscopes are faster (1GHz bandwidth) and come with a wide variety of mixed signal, serial data, long memory and probe options and accessories.

The HDO8000 is ideal for high-power three-phase power electronics system analysis, in a power electronics market that is growing quickly, especially in high-power and three-phase energy conversion applications focused on distributed power generation (solar PV, wind, etc) and hybrid electric and electric (HEV and EV) vehicle propulsion systems. New and expanded efficiency requirements for electric motors and variable frequency (motor) drives are also driving higher demand for three-phase power electronics.

HD4096 technology incorporates low-noise system architecture, high-sample-rate 12-bit ADCs and high signal-to-noise ratio amplifiers, enabling the oscilloscopes to capture and display signals of up to 1GHz with high sample rate and 16 times more resolution compared to others.

www.teledynelecroy.com

NEW DUAL-OUTPUT DIFFERENTIAL SPEED AND DIRECTIONAL SENSOR IC

The new ATS605 from Allegro MicroSystems Europe is a dual-output speed and direction sensing IC sensor designed for use in rotational position sensing applications in conjunction with a ferrous gear target.

The ATS605 incorporates three Hall sensing elements used to create two independent differential channels. Signals from these channels are then processed by the IC, which contains a sophisticated digital circuit designed to eliminate the detrimental effects of magnet and system offsets. The differential signals are used to produce highly accurate speed output and, if desired, provide information on the direction of rotation.

Advanced calibration techniques are used to optimise signal offset and amplitude. This calibration, combined with the digital tracking of the signal, results in accurate switch-points over different air gaps and temperature. The open-drain outputs provide voltage output signals which mirror the sensed target's shape, with a phase separation between the two channels proportional to the size of the target teeth compared with the Hall element spacing.

www.allegromicro.com

LORD LIEUTENANT OF HAMPSHIRE VISITS HARWIN'S PORTSMOUTH FACTORY

Harwin's Portsmouth factory received an official visit from the Lord Lieutenant of Hampshire, Dame Mary Fagan (pictured) last month. Dame Mary was welcomed on arrival by Harwin Chairman, Damon de Laszlo (pictured), before meeting Harwin's design and engineering teams.

Dame Mary was taken on a tour of Harwin's factory, where its high-reliability connectors, including the triple award-winning Gecko G125 Series are manufactured, as well as its EZ-Boardware PCB hardware products. Dame Mary talked with technicians involved in the many processes involved in producing the company's connectors which are used in applications as diverse as medical devices, satellites, aircraft and high-end autosport including Indy cars.

One of the highlights of the visit was a certificate presentation ceremony; Dame Mary congratulated Andrew McGuinness, Sam Bennett and Ethan Mew (all pictured), who have just completed four-year Advanced Level Apprenticeships and presented them with their certificates.

www.harwin.co.uk

DRIVER REFERENCE DESIGNS FOR CREE LED BULBS

Power Integrations announced four reference designs describing drivers for dimmable PAR 30 and PAR 38 LED lightbulbs. Jointly developed with CREE, the designs showcase the combination of Power Integrations's LYTSwitch-4 driver ICs and CREE MT-G2 EasyWhite LEDs. DER-364 and DER-365 detail low- and high-line PAR 30 LED bulb drivers, respectively, while DER-350 and DER-396 address low- and high-line PAR 38 bulbs.

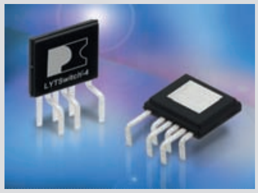

LYTSwitch-4 ICs are highly efficient and deliver accurate output current regulation in bulb and tube replacement applications and high-bay lighting. The devices simplify design and reduce cost while ensuring that lamps deliver uniform light output and provide exceptional performance in TRIAC-dimmable applications. LYTSwitch-4 ICs combine PFC and constant current in a single-stage topology, resulting in power factor greater than 0.95 and typical efficiencies of better than 90%. The single-stage approach also eliminates temperature-sensitive electrolytic bulk capacitors, greatly increasing the bulbs' reliability and lifetime.

www.powerint.com/ledrivers/cree

TTI DELIVERS FULL M8/M12 CONNECTOR SYSTEM FROM TE CONNECTIVITY

TTI Inc now offers TE Connectivity's (TE) complete M8/M12 connector system for machine industrial automation and control applications.

TE's M8/M12 system includes an extensive portfolio of connectivity solutions, including a full range of PCB headers, cable assemblies and I/O boxes, and provides users with a future-proof interface that supports higher bandwidth needs. The system meets industrial automation speed requirements of up to 10Gb/s and ensures reliable communication in harsh industrial environments.

Norbert Piefer, TTI's marketing director of Industrial in Europe explained: "In addition to TE's connectors, we now offer all the accessories and system-level components such as M8/M12 distribution boxes as part of our new strategic industrial relationship with TE. This system enables installers to bundle 4, 6, 8 or 12 connector pairs into one neat, convenient I/O package."

Typical applications for the M8/M12 system include sensors to detect movement, proximity, level and motion, as well as actuators to control motors, valves, solenoids and lighting.

www.ttieurope.com

AVX EXTENDS THE CAPACITANCE RANGE FOR ITS X7R MLCCs

AVX Corporation has extended the capacitance range and voltage ratings for its X7R MLCCs, resulting in a much broader product offering with several new high volumetric efficiency options. Available in sizes spanning 01005 to 2225, AVX's X7R MLCCs exhibit high K and low ESR and are now available with capacitance values spanning 100pF to 47µF and standard voltage ratings spanning 4V-500V. High voltage X7R MLCCs with ratings up to 5000V are also available, as are automotive and alternate termination options.

Ideal applications for X7R MLCCs include decoupling and filtering in mobile, medical and digital applications, such as cell phones, tablets, high-speed processors/FPGAs and implantable medical devices, in which high volumetric efficiency is especially critical. The series is also particularly well suited for use as snubbers, resonators, filters, or DC blocking caps in automotive, medical, industrial and commercial electronics, including displays, high voltage multipliers, high-frequency power converters and SMPS.

www.avx.com

GAN SYSTEMS'S JULIAN STYLES ELECTED TO THE BOARD OF PEIC IN THE US

GaN Systems announced that Julian Styles, Director of Business Development USA, has been elected to the Board of the Power Electronics Industry Collaborative (PEIC), the US industry consortium of suppliers, OEMS, stakeholders and research companies committed to accelerating development and growth of power electronics in the US.

PEIC's aim is to increase investment in manufacturing capabilities and advance innovation in power electronics in the US as energy efficiency becomes ever more important globally.

"We are thrilled that GaN Systems has joined PEIC's Board of Directors," said PEIC Board President, Mark Bellinger. "Julian's expertise is extremely valuable and he will certainly be a great addition to the Board."

GaN Systems has developed a range of gallium nitride power switching products based on its proprietary Island Technology. The company's devices overcome the limitations of traditional silicon semiconductors, offering far greater efficiency in power conversion applications such as solar, wind, smart-grid, electric and hybrid vehicles and power supply applications.

www.gansystems.com

SONDREL TAKES SECURITY TO A NEW LEVEL

Sondrel, a system-to-silicon IC design consultancy, is employing secure border computing technology from Zentera Systems to ensure IP protection with the minimum of impact on its customers' IT infrastructure.

Zentera's Hybrid Cloud Technologies enable IP to be securely accessed from diverse worldwide locations, ensuring that the best available design resources can be employed to get the project done on time at the best performance. Using Zentera's secure border computing technology also ensures access to customers' IP can be subject to detailed control and monitoring.

Sondrel provides outsourced design services to many leading companies and has design centres in multiple locations including the US, Europe, China, Scandinavia and Israel. The company works in collaborative partnership with its customer base so it is vital that sensitive and valuable IP can be accessed securely and easily.

Sondrel wants to offer additional security assurance to its customers and Zentera technology due to the strength and flexibility of its hybrid cloud solutions.

www.sondrel.com

COLOUR CODING OF NEW BINDER M12 PANEL MOUNT CONNECTORS AVOIDS COSTLY ERRORS

Binder has introduced a new range of M12, A-coded panel mount connectors that have colour-coded inserts to help prevent incorrect mating. Black, purple, orange, yellow, green, red and blue inserts are available in four- and five-pole format and in both male and female rear-mounting versions; the mounting thread is M16.

Ideal for applications in control, automation, sensing and instrumentation equipment, the connectors are pre-wired with 200mm diameter wire as standard and alternative lengths are available on request as are dip-solder contacts for PCB mounting.

Protected to IP67 when mated, these new connectors have a body made from nickel-plated brass, male contacts are gold plated while the female contacts are brass and life is in excess of 100 mating cycles.

Based in Hemel Hempstead, Binder UK is the subsidiary of Franz Binder GmbH, the manufacturer of circular and other connector products that serves the instrumentation, sensor, automation, medical and industrial equipment markets.

www.binder-connector.co.uk

NEW PROVERTHA M12 CONNECTORS FROM AERCO

Now available from Aerco is the Provertha range of Profinet and Ethernet I-Net M12 connectors, ideal for demanding applications such as the rail industry.

Reliable and robust with a simple, fail-safe connection, these A and D coded 4, 5 and 8 pin connectors provide 360° EMI/RFI shielding, and are protected to IP67 and provide fault-free data transmission. The compact design allows fast and easy assembly even where space is restricted and is ideal for fast and reliable connection for field applications.

The high-quality, robust metal housing and a crimp-flange system provide the torsion-resistant strain relief required for tough industrial environments. Safe signal contact is ensured with high quality crimp contacts and waterproof clamp flange.

These new M12 connectors can be are supplied in various formats for I-Net Profibus bus systems and conventional cable and panel-mounted versions.

www.aerco.co.uk

HAN CONNECTORS WITH RFID TECHNOLOGY OFFER ADDED VALUE

Harting's family of Han industrial connectors are now equipped with RFID transponders, enabling specific data on the connector configuration to be linked with factory IT systems to aid processes such as the ordering of spare parts.

Han connector systems offer optimum protection against external physical influences, made possible by the use of materials and seals that are UV and ozone resistant and which function over a temperature range from -40°C to +125°C.

Impermeability to moisture, humidity, dust and dirt is also assured throughout the connectors' life, with both connectors and RFID transponders designed to meet the requirements of IP 65/67 on moisture protection.

The integration of RFID transponders into the rectangular Han connectors allows the development and use of the full range of identification data and its integration into business database structures, including the ordering of spare parts, all in a convenient, quick and reliable manner.

www.harting.com

INTELLICONNECT EXTENDS PISCES RANGE OF WATERPROOF CONNECTORS

Intelliconnect (Europe) Ltd has extended its Pisces range of IP68 waterproof connectors to include additional connector and cable termination options. The range now includes SMA, TNC and N Type cable plug options which may be connected to a wide variety of cables including many LMR, RG, semi-rigid and semi-flexible cable types.

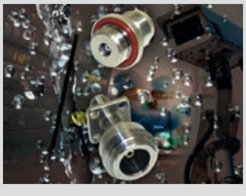

These product enhancements extend the range of potential applications for Pisces connectors to include 75-ohm variants for video camera security applications, environmental monitoring ocean buoys, traffic cameras (ANPR), coastguard/HM customs patrol boats, military radios/communication systems, environmental monitoring and water management and vehicle tracking.

In addition to Intelliconnect's renowned fast turnaround custom-design connector service its extensive standard range includes IP67 and IP68 rated interconnect solutions for harsh environments including N Type, SMC, SMA, TNC, push-pull and ABMS (harsh environment MCX). The SSMA is a smaller version of SMA which provides higher frequency performance.

www.intelliconnect.co.uk

CLIFF ELECTRONICS EXPANDS SPACE SAVING RANGE OF USB DATA SOCKETS

Cliff Electronics has extended its range of space-saving Digital XLR connectors. Mounted in an industry standard XLR connector shell, the Cliff Digital XLR range offers highly efficient use of panel space and the manufacturing convenience of making the same panel cut-out for all analogue and digital connector requirements.

USB data connection to audio, broadcast, AV (audio-visual), lighting controllers, instrumentation and industrial equipment is becoming more common as digital signal and control options increase and more information needs to be transferred between portable equipment, smart phones, tablets and other data storage devices which can also be powered or charged while connected.

The recent introduction of the unique Cliff Dual USB2 connector, which provides two isolated and independent fully USB compliant sockets in a panel space-saving single XLR receptacle, has generated demand for further variants, so a further two new Digital XLR connector types have now been introduced: USB2 gender changer feed-through sockets available as either USB2 A to B or B to A versions.

www.cliffuk.co.uk

QUICK AND RELIABLE CONNECTION TO LED CHIP-ON-BOARD ARRAY HOLDERS

Molex has added to its portfolio Plastic Substrate Interconnect (PSI) for LED Chip-on-Board (CoB) Arrays. These customisable interconnects feature a low-profile harness interface that delivers power to the array through a simple and reliable connection to a holder, or plastic substrate. With a low overall package height of ~ 2.00mm, Molex PSI provides a slim design for space-limited applications while minimising substrate costs. By employing the Pico-EZmate harness system, the solution integrates the electrical and mechanical features with the array for a simple, solderless connection.

The PSI system is ideal for high-density and high-light output applications such as down lighting (track, pendants and linear) and area lighting (carriageways, car parks and wall packs). LED Chip-on-Board technology ensures strong future development capabilities by allowing integration of additional components. The system supports a variety of potential PSI designs including circular, rectangular as well as customisable shapes and receptacles.

www.molex.com

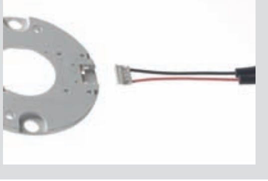

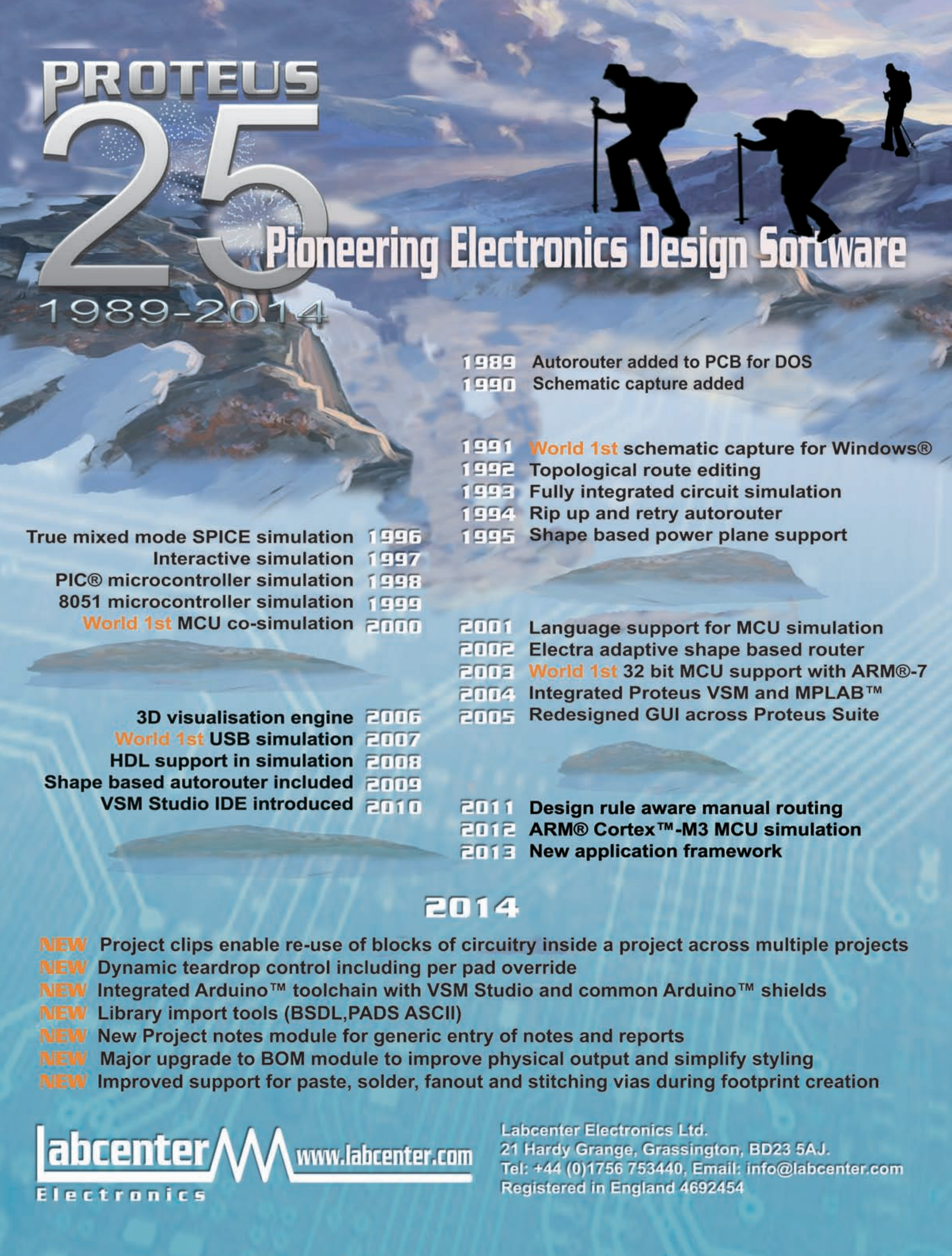
PROTEUS
25
Pioneering Electronics Design Software
1989-2014
1989 Autorouter added to PCB for DOS
1990 Schematic capture added
1991 World 1st schematic capture for Windows®
1992 Topological route editing
1993 Fully integrated circuit simulation
1994 Rip up and retry autorouter
1995 Shape based power plane support
True mixed mode SPICE simulation 1996
Interactive simulation 1997
PIC® microcontroller simulation 1998
8051 microcontroller simulation 1999
World 1st MCU co-simulation 2000
2001 Language support for MCU simulation
2002 Electra adaptive shape based router
2003 World 1st 32 bit MCU support with ARM®-7
2004 Integrated Proteus VSM and MPLAB™
2005 Redesigned GUI across Proteus Suite
3D visualisation engine 2006
World 1st USB simulation 2007
HDL support in simulation 2008
Shape based autorouter included 2009
VSM Studio IDE introduced 2010
2011 Design rule aware manual routing
2012 ARM® Cortex™-M3 MCU simulation
2013 New application framework
2014
NEW Project clips enable re-use of blocks of circuitry inside a project across multiple projects
NEW Dynamic teardrop control including per pad override
NEW Integrated Arduino™ toolchain with VSM Studio and common Arduino™ shields
NEW Library import tools (BSDL,PADS ASCII)
NEW New Project notes module for generic entry of notes and reports
NEW Major upgrade to BOM module to improve physical output and simplify styling
NEW Improved support for paste, solder, fanout and stitching vias during footprint creation
labcenter Electronics
www.labcenter.com
Labcenter Electronics Ltd.
21 Hardy Grange, Grassington, BD23 5AJ.
Tel: +44 (0)1756 753440, Email: info@labcenter.com
Registered in England 4692454

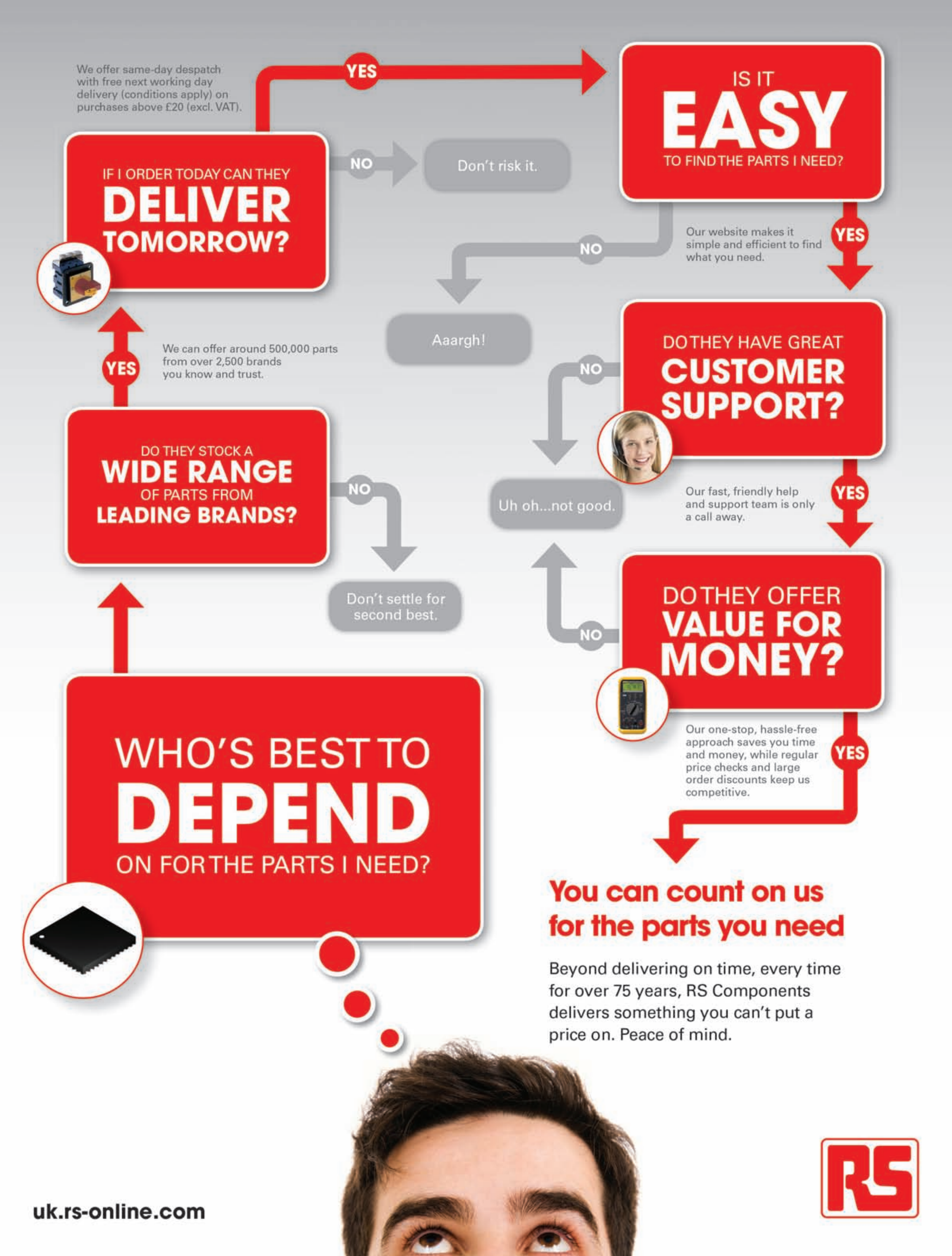
WHO'S BEST TO
DEPEND
ON FOR THE PARTS I NEED?
DO THEY STOCK A
WIDE RANGE
OF PARTS FROM
LEADING BRANDS?
NO
Don't settle for second best.
YES
We can offer around 500,000 parts from over 2,500 brands you know and trust.
IF I ORDER TODAY CAN THEY
DELIVER
TOMORROW?
NO
Don't risk it.
YES
We offer same-day despatch with free next working day delivery (conditions apply) on purchases above £20 (excl. VAT).
IS IT
EASY
TO FIND THE PARTS I NEED?
NO
Aaargh!
YES
Our website makes it simple and efficient to find what you need.
DO THEY HAVE GREAT
CUSTOMER
SUPPORT?
NO
Uh oh...not good.
YES
Our fast, friendly help and support team is only a call away.
DO THEY OFFER
VALUE FOR
MONEY?
NO
YES
Our one-stop, hassle-free approach saves you time and money, while regular price checks and large order discounts keep us competitive.
You can count on us for the parts you need
Beyond delivering on time, every time for over 75 years, RS Components delivers something you can't put a price on. Peace of mind.
uk.rs-online.com
RS